Crosstalk between the muscular estrogen receptor α and BDNF/TrkB signaling alleviates metabolic syndrome via 7,8-dihydroxyflavone in female mice

Zhenlei Zhao [1], Fan Xue [1], Yanpei Gu [1], Jianxin Han [1], Yingxian Jia [2], Keqiang Ye [3],**, Ying Zhang [1],*

ABSTRACT

Objective: 7,8-Dihydroxyflavone (7,8-DHF), a small molecular mimetic of brain-derived neurotrophic factor (BDNF), alleviates high-fat diet-induced obesity in female mice in a sex-specific manner by activating muscular tropomyosin-related kinase B (TrkB). However, the underlying molecular mechanism for this sex difference is unknown. Moreover, muscular estrogen receptor α (ERα) plays a critical role in metabolic diseases. Impaired ERα action is often accompanied by metabolic syndrome (MetS) in postmenopausal women. This study investigated whether muscular ERα is involved in the metabolic effects of 7,8-DHF.

Methods: For the *in vivo* studies, 72 female C57BL/6J mice were given a low-fat diet or high-fat diet, and both received daily intragastric administration of vehicle or 7,8-DHF for 24 weeks. The hypothalamic-pituitary-ovarian (HPO) axis function was assessed by investigating typical sex-related serum hormones and the ovarian reserve. Indicators of menopausal MetS, including lipid metabolism, insulin sensitivity, bone density, and serum inflammatory cytokines, were also evaluated. The expression levels of ERα and other relevant signaling molecules were also examined. *In vitro*, the molecular mechanism involved in the interplay of ERα and TrkB receptors was verified in differentiated C2C12 myotubes using several inhibitors and a lentivirus short hairpin RNA-knockdown strategy.

Results: Long-term oral administration of 7,8-DHF acted as a protective factor for the female HPO axis function, protecting against ovarian failure, earlier menopause, and sex hormone disorders, which was paralleled by the alleviation of MetS coupled with the production of ERα-rich, TrkB-activated, and uncoupling protein 1 (UCP1) high thermogenic skeletal muscle tissues. 7,8-DHF-stimulated transactivation of ERα at serine 118 (S118) and tyrosine 537 (Y537), which was crucial to activate the BDNF/TrkB signaling cascades. In turn, activation of BDNF/TrkB signaling was also required for the ligand-independent activation of ERα, especially at the Y537 phosphorylation site. In addition, Src family kinases played a core role in the interplay of ERα and TrkB, synergistically activating the signaling pathways related to energy metabolism.

Conclusions: These findings revealed a novel role of 7,8-DHF in protecting the function of the female HPO axis and activating tissue-specific ERα, which improves our understanding of this sex difference in 7,8-DHF-mediated maintenance of metabolic homeostasis and provides new therapeutic strategies for managing MetS in women.

1. INTRODUCTION

Metabolic syndrome (MetS) is a major public health problem worldwide and is characterized by a cluster of metabolic abnormalities, including obesity, visceral adiposity, hyperinsulinemia, hyperglycemia, hyper-cholesterolemia, and hypertension [1,2]. Sex differences in obesity and MetS are observed frequently in both animals and humans [3—7];

however, the underlying mechanisms have remained enigmatic. In fact, the incidences of insulin resistance and type 2 diabetes (T2D) are higher in men than in similarly aged premenopausal women [7,8]. Unfortunately, following the onset of menopause, women are more vulnerable to developing metabolic-related chronic diseases, such as abdominal obesity, insulin resistance, and even T2D [9,10]. Increasing evidence suggests that the hypothalamic pituitary ovarian (HPO) axis-

[1]Department of Food Science and Nutrition, School of Biosystems Engineering and Food Science, Zhejiang Key Laboratory for Agro-Food Processing, Zhejiang Engineering Center for Food Technology and Equipment, Zhejiang University, Hangzhou 310058, China [2]Department of Gynecology, Women's Hospital, Zhejiang University School of Medicine, Hangzhou 310058, China [3]Department of Pathology and Laboratory Medicine, Emory University School of Medicine, Atlanta, GA 30322, USA

*Corresponding author. Department of Food Science and Nutrition, School of Biosystems Engineering and Food Science, Zhejiang University, #866 Yuhangtang Road, Hangzhou 310058, China. E-mail: yzhang@zju.edu.cn (Y. Zhang).

**Corresponding author. Department of Pathology and Laboratory Medicine, Emory University School of Medicine, 100 Woodruff Circle, Atlanta, GA 30322, USA. E-mail: kye@emory.edu (K. Ye).

Original Article

regulated sex hormones and their receptors, especially the activities of estrogen and estrogen receptors, contribute to this process. In humans, together with estrogen (E2) deficiency, a high circulating follicle-stimulating hormone (FSH) level occurs in response to ovarian failure and is regarded as a marker for the onset of menopause [11,12]. Although numerous studies have confirmed that reductions in estrogen action promote metabolic dysfunction, which predisposes to obesity and MetS [13,14], the tissue-specific molecular actions of estrogen and its receptor in metabolic tissues require further study.

Estrogen receptors, mainly comprising estrogen receptor alpha (ERα) and estrogen receptor beta (ERβ), are members of the nuclear receptor superfamily of ligand-regulated transcription factors [15,16] and are widely expressed in many cells and tissues, such as the ovary, hypothalamus, muscle, adipocytes, and bone [17]. Skeletal muscle is responsible for 75—85% of insulin-induced glucose disposal, which involves estrogen receptors [18,19]. ERα is the most abundant estrogen receptor expressed in skeletal muscle and is believed to be a vital signal molecule involved in skeletal muscle oxidative metabolism and glucose uptake [20—22]. A previous study demonstrated that a reduced expression level of the muscle ERα gene (*ESR1/Esr1*) is implicated in metabolic dysfunctions and increased adiposity in women and female mice [20]. In contrast, activation of muscular ERα by its agonist resveratrol could enhance muscular glucose uptake and alleviate diet-induced insulin resistance syndrome [23]. Accordingly, restoring ERα expression or activity might represent a potential therapeutic strategy to treat MetS [19].

Brain-derived neurotrophic factor (BDNF) is a member of the neurotrophin family that plays an important role in synaptic plasticity, neuronal survival, neuronal development, and differentiation [24]. BDNF binds to the receptor tyrosine kinase B (TrkB) and triggers TrkB autophosphorylation, which subsequently activates several downstream signaling cascades, including the RAS mitogen-activated protein kinase (MAPK)/ERK kinase (MEK)-extracellular regulated kinase (ERK) and phosphatidylinositol-4,5-bisphosphate 3-kinase (PI3K)/protein kinase B (AKT) pathways [25—27]. Generally, BDNF/TrkB signaling is required in the central nervous system (CNS) for a variety of neuronal functions, including neurotransmission and synaptic plasticity [28,29]. Previous studies also revealed a novel non-neurotrophic function of BDNF, in which it acts as an anorexic factor on hypothalamic neurons and thus reverses eating behavior and obesity [30,31]. Yang et al. [32] revealed that muscle-derived BDNF acts as a myokine and plays an important role in controlling energy metabolism. However, the clinical application of BDNF is greatly limited by its short half-life and non-bioavailable nature [33]. As an orally bioavailable BDNF mimetic, plant-derived 7,8-dihydroxyflavone (7,8-DHF) has been identified as a specific TrkB agonist that induces TrkB dimerization and activates its downstream signaling molecules, including AKT and ERK [34]. 7,8-DHF has been studied widely [35,36], mainly focusing on treating CNS-related diseases, such as Alzheimer's disease, cognitive dysfunction, depression, and Parkinson's disease [36—39]. However, there are only a few reports concerning the role of 7,8-DHF in treating peripheral tissue-related metabolic diseases [40,41]. We recently showed that 7,8-DHF treatment plays both preventive and therapeutic roles in the development of high-fat diet (HFD)-induced obesity; however, this is only valid in female mice, and the activation of BDNF/TrkB signaling in skeletal muscle appears to be the main pathway involved [42,43]. Nevertheless, the mechanism underlying this sex difference is unknown. Previous research showed that female-specific induction of ERα expression confers neuroprotection when combined with 7,8-DHF-induced activation of TrkB in female neonates after hypoxia and ischemia encephalopathy [44]. Therefore, we investigated whether ERα is involved in the 7,8-DHF-stimulated activation of BDNF/

TrkB signaling cascades in muscles, thus improving MetS in mature adult female mice.

The results of this study revealed a protective effect of 7,8-DHF on the hypothalamic-pituitary-ovarian (HPO) axis function as well as the key role of muscular ERα and its interaction with the BDNF/TrkB signaling pathway for skeletal muscle energy metabolism. Taken together, our findings might contribute to a sex-specific alleviation of MetS, allowing the development of effective interventions for human metabolic dysfunction in women.

2. MATERIALS AND METHODS

2.1. Animals and study design

A total of 72 eight-week-old C57BL/6J female mice were purchased from Shanghai Sippr-BK Laboratory Animal Co., Ltd. (Shanghai, China). All of the animal experiments were approved by the Institutional Animal Care and Use Committee (IACUC) of Zhejiang Chinese Medical University (approval no.: IACUC-20180514-03). Animal care was given in accordance with institutional guidelines. The mice were housed in environmentally controlled conditions with a 12-h light/dark cycle and free access to water and food. The HFD (60 kcal% fat, D12492) and LFD (10% kcal%, D12450J) were purchased from Research Diets, Inc. Co., Ltd. (New Brunswick, NJ, USA). After one week of acclimation, the mice were randomly divided into six groups (n = 12 per group; n = 4 per cage) and fed different diets as follows: (1) LFD control group; (2) LFD with 7,8-DHF at a medium dose of 10 mg/kg·BW (LFD+DHF$_{10}$); (3) HFD control group; (4) HFD with 7,8-DHF at a low dose of 5 mg/kg·BW (HFD+DHF$_5$); (5) HFD with 7,8-DHF at a medium dose of 10 mg/kg·BW (HFD+DHF$_{10}$); and (6) HFD with 7,8-DHF at a high dose of 20 mg/kg·BW (HFD+DHF$_{20}$). The mice in every group received vehicle or 7,8-DHF dissolved in 5% DMSO/0.5% methylcellulose at a low, medium, and high dose by intragastric administration. Body weight and food intake were recorded weekly during the experiments. After 16 weeks of feeding (24 weeks of age), the estrus cycle stage in each group was assessed daily (9.00−11.00 a.m.) until there was an obvious difference in the estrus frequency between the 7,8-DHF treated groups and control groups. Each mouse cycle typically lasts 4−5 days, including proestrus, estrus, metestrus, and diestrus [45]. The estrus cycle stage was determined by the cytological analysis of vaginal smears according to a previously reported method [46]. At the end of the dietary intervention, the fasted mice were anaesthetized and killed by cervical dislocation and blood samples were collected. Tissues were harvested and weighed and then fixed with 4% paraformaldehyde or snap-frozen in liquid nitrogen and stored at −80 °C until further use. Glucose tolerance tests (GTTs) and insulin tolerance tests (ITTs) were performed before sacrifice. The mice used for the GTTs were fasted overnight and given glucose intraperitoneally (2 g/kg·BW), and blood glucose was measured in the tail vein blood at 0, 30, 60, 90, and 120 min using an ACCU-CHEK Blood Glucose Meter (Roche, Basel, Switzerland). Similarly, the ITT was performed on the mice after peritoneal injection of recombinant human insulin (0.75 U/kg, Novo Nordisk, Bagsvaerd, Denmark).

2.2. Biochemical analyses

The blood glucose level was measured using an ACCU-CHEK Advantage Blood Glucose Meter (Roche). Serum concentrations of triacylglycerol (TG), free fatty acid (FFA), and total cholesterol (T-CHO) were determined using commercially available kits (Jiancheng, Nanjing, China) based on the manufacturer's instructions. Serum levels of endotoxin lipopolysaccharide (LPS), tumor necrosis factor α (TNF-α), interleukin-6 (IL-6), anti-Müllerian hormone (AMH), and FSH

were detected using mouse ELISA kits (Cusabio Biotech Co., Ltd., Wuhan, China); serum insulin and E2 levels were assessed using ELISA kits from Shanghai Westang Bio-Tech Co., Ltd. (Shanghai, China).

2.3. Micro-computed tomography (micro-CT)

Imaging and quantification of fat volume in thoracolumbar compartments were conducted using micro-CT (NEMO Micro-CT, Pingsheng Healthcare Shanghai Inc., Shanghai, China) following a previously reported protocol [11,47]. Briefly, the mice were anaesthetized with 5% isoflurane and O$_2$ for 5−10 min and subjected to CT scans with a detector size of 1944 × 1536 pixels. The torso of each mouse was scanned at an isotropic voxel size of 80 μm (65 kV, 190 μA). Two-dimensional grayscale image slices were reconstructed into 3D tomograms using commercial image-processing software (Recon, Pingsheng, Shanghai, China). Three-dimensional (3D) segmentation of fat was performed between the upper edge of the pulmonary and end of the femur. The head and feet were excluded because of the relatively low adiposity in these regions. A thresholding technique was applied to all of the images to separate the fat. Fat regions were manually traced using the thresholding technique. Quantification of the volume of subcutaneous WAT (sWAT) and visceral WAT (vWAT) was obtained through 3D reconstruction software using iterative algorithms.

Bone mineral density measurements were also performed on the mice after calibration by a standard bone density phantom (QRM-Micro-CT-HA, Möhrendorf, Germany) [48]. The TBD (including neither the region above the cervical spine nor below the caudal vertebra) and region-specific bone mineral density, including SBD (the region between the cervical spine and caudal vertebra) and FBD were also determined. The instrument was calibrated each time before use by employing a phantom pass according to the manufacturer's recommendation. Three-dimensional models of these bones were then reconstructed using 3D reconstruction software (Recon).

2.4. Ovarian histology and follicle counts

The number of follicles was estimated according to previous reports [49,50]. In brief, ovaries were fixed (4% paraformaldehyde), paraffin embedded, and serially sectioned (5 μm thick) throughout the entire ovary, aligned in order on glass microscope slides, and stained with hematoxylin and eosin (H-E). The numbers of primordial follicles (Pr), primary follicles (P), secondary follicles (S), healthy antral follicles (A), and atretic follicles (Af) in every fifth section (spaced at 20 μm) with a random start were then determined as previously detailed [49,51,52]. Because this procedure samples one-fifth of the entire ovarian volume, the total number of follicles per ovary was then estimated by multiplying the cumulative counts for each ovary by a correction factor of five [50].

2.5. Histological analysis

Freshly isolated tissues (inguinal adipose tissue, liver, and ovary) were selected and fixed in 4% neutral formaldehyde solution for 24 h. All of the tissues were dehydrated in graded ethanol (30, 50, 70, 80, 95, and 100% ethanol) for 45 min each, followed by paraffin-embedded sectioning and H-E staining. Histological observation was performed using a binocular microscope (Eclipse E100, Nikon, Tokyo, Japan).

2.6. Cell culture and glucose consumption experiments

Mouse C2C12 myoblasts were cultured in Dulbecco's modified Eagle's medium (DMEM) with 10% fetal bovine serum, 100 I.U./mL penicillin, and 100 μg/mL streptomycin (Invitrogen, Waltham, MA, USA) at 37 °C

with 95% air and 5% CO_2. To induce differentiation, cells were incubated until 100% confluent and switched to differentiation medium DMEM (2% horse serum, 100 I.U./mL penicillin, and 100 μg/mL streptomycin) for 4—6 days [43]. To treat differential C2C12 myotubes, 7,8-DHF was dissolved in DMSO to produce a 200 mM stock solution and subsequently diluted with cell culture medium to different concentrations (final concentration of DMSO < 0.1%). For the glucose consumption assays, cells were cultured and differentiated on 48-well cluster dishes. After the differentiation process was complete, C2C12 myotubes were incubated in differentiation media with various concentrations of 7,8-DHF (0, 0.5, 1.0, or 5.0 μmol/L) or BDNF (0, 50, 100, or 200 ng/mL) for 16 h, and the supernatant was then collected in 1.5 mL centrifuge tubes for testing. Glucose consumption was measured using a Glucose Assay Kit (Applygen Technologies, Inc., Beijing, China) based on the glucose oxidase method in accordance with the manufacturer's protocol. In some experiments, cells were preincubated with ICI182780 (1 μmol/L, an inhibitor of the estrogen receptor) or k252a (30 nmol/L, an inhibitor of TrkB) for 30 min at 37 °C before treatment with 7,8-DHF or BDNF.

2.7. Quantitative real-time reverse transcription PCR
Levels of mRNA were analyzed using qRT-PCR. Total RNA was isolated from tissues using TRIzol (Invitrogen) and reverse transcribed into cDNA using an RT reagent kit (Takara Bio Inc., Shiga, Japan) according to the manufacturer's instructions. Gene-specific primers were synthesized by Shenggong Bioengineering Technology Limited (Shanghai, China) and are listed in Supplemental Table 1. All of the quantitative real-time PCR reactions were performed using a LightCycler 480 II Real-Time PCR Detection System (Roche). The relative quantification of gene expression was calculated using the $2^{-\Delta\Delta Ct}$ method [53]. The housekeeping gene *Ppia* (encoding peptidylprolyl isomerase A) was used as a control.

2.8. Western blotting
Tissues or cells were homogenized in radioimmunoprecipitation assay (RIPA) lysis buffer (P0013B, Beyotime, Beijing, China) with protease and phosphatase inhibitor cocktail (P1045, Beyotime) on ice. Cell debris was removed by centrifugation at $14,000 \times g$ for 5 min at 4 °C. The protein extract was diluted to 2—4 mg/ml. Thirty to forty micrograms of total protein per sample were electrophoresed and then transferred onto a polyvinylidene fluoride (PVDF) membrane (Bio-Rad Laboratories, Hercules, CA, USA). Membranes were blocked with Tris-buffered saline tween containing 5% skim milk powder for 2 h at room temperature and subsequently incubated overnight at 4 °C with the recommended amount of primary antibody, followed by incubation with secondary antibodies and visualization of the immunoreactive protein bands. The levels of phosphorylated proteins were normalized to the levels of their corresponding total proteins unless specifically noted, and the proteins were normalized to the internal controls (GAPDH or tubulin). For some experiments, membranes were stripped in Western stripping buffer (Pulilai Gene Technology Co., Ltd., Beijing, China) and re-probed with different antibodies.

2.9. Lentiviral-induced *Esr1* knockdown in C2C12 myoblasts
To achieve *Esr1* (mouse ERα gene) knockdown (KD) in C2C12 myoblasts, lentiviral particles carrying shRNAs targeted to *Esr1* or the respective controls were obtained from Hanbio Biotechnology Co., Ltd. (Shanghai, China). Referring to a previous study [20], three potential shRNAs (Esr1-KD1, Esr1-KD2, and Esr1-KD3) and one control shRNA (Esr1-con) were designed and synthesized; the sequences are listed in Supplemental Table 2. Lentivirus transduction was performed

using polybrene transfection reagent and a green fluorescent protein (GFP) plasmid was used to measure and confirm the transfection efficiency (Supplemental Figure 1). After selecting positive transformants using puromycin (Dalian Meilun Biotechnology Co., Ltd., Dalian, China), the selected clones were expanded and analyzed for their KD efficiency as measured using qRT-PCR and immunoblotting. The resulting cultures were then differentiated and used for subsequent assays.

2.10. Materials
C2C12 cells were purchased from ATCC (Manassas, VA, USA) and maintained as instructed. 7,8-DHF (purity > 98%) was purchased from Tokyo Chemical Industry Co., Ltd. (Tokyo, Japan). BDNF (AF-450-02, purity ≥ 98%) was obtained from Proteintech Group, Inc. (Rosemont, IL, USA). Estrogen receptor antagonist ICI182780 (T2146, purity > 99%), specific Src inhibitor PP1 (T6196, purity > 99%), and SCH772984 (T6066, purity > 99%) were purchased from Topscience Co., Ltd. (Shanghai, China). K252a (#12754, purity > 99%), antibodies against Src (#2108), p-Src Tyr416 (#2101), ERK (#9102), p-ERK (Thr202/Tyr204) (#9106), pan AKT (#4691), and p-AKT S473 (#4060) were obtained from Cell Signaling (Danvers, MA, USA). Anti-ERα (ab32063), p-ERα Ser118 (ab32396), and UCP1 (ab155117) antibodies were purchased from Abcam (Cambridge, MA, USA). Anti-TrkB (AF6461), p-TrkB Tyr706 (AF3461), α-tubulin (AF7010), and glyceraldehyde-3-phosphate dehydrogenase (GAPDH) (AF7021) were purchased from Affinity Biosciences (Cincinnati, OH, USA). Anti-p-ERα Tyr537 (#PA5-104732) antibodies were obtained from Thermo Fisher Scientific (Waltham, MA, USA).

2.11. Statistical analysis
All of the data obtained from three or more independent experiments were expressed as mean ± SD and analyzed using GraphPad Prism statistical software (GraphPad Software, Inc., La Jolla, CA, USA). All of the statistical details on the experiments can be found in the figure legends for each experiment, including the statistical tests used, number of mice in the animal experiments (represented as n unless otherwise stated), and number of wells in the cell culture experiments (represented as n unless otherwise stated). Differences between two groups were assessed using an unpaired two-tailed Student's t test. For more than two groups, one-way analysis of variance (ANOVA) was applied to assess the statistical significance. $P < 0.05$ was considered statistically significant.

3. RESULTS

3.1. Long-term 7,8-DHF treatment inhibited HFD-induced weight gain and adiposity and increased bone mineral density in female mice
A previous study showed that 7,8-DHF selectively prevents body weight gain in female mice vs male mice [42]. To explore whether 7,8-DHF also influences other sex-related biological features, we treated the mice with LFD or HFD in the presence of different doses of 7,8-DHF. To obtain accurate data on the distribution of thoracoabdominal white adipose tissue (WAT), micro-computed tomography (micro-CT) was adopted. Micro-CT of distinct thoracoabdominal WAT compartments revealed a substantial increase in both the total fat volume (TFV), subcutaneous fat volume (SFV), and visceral fat volume (VFV) in the HFD-fed control group vs the LFD-fed control group (Figure 1A). In the groups fed an LFD, no obvious differences in the TFV, SFV, and VFV were observed after treatment with 7,8-DHF. In contrast, the TFV, SFV, and VFV were all significantly reduced ($p < 0.01$) in the 7,8-DHF-
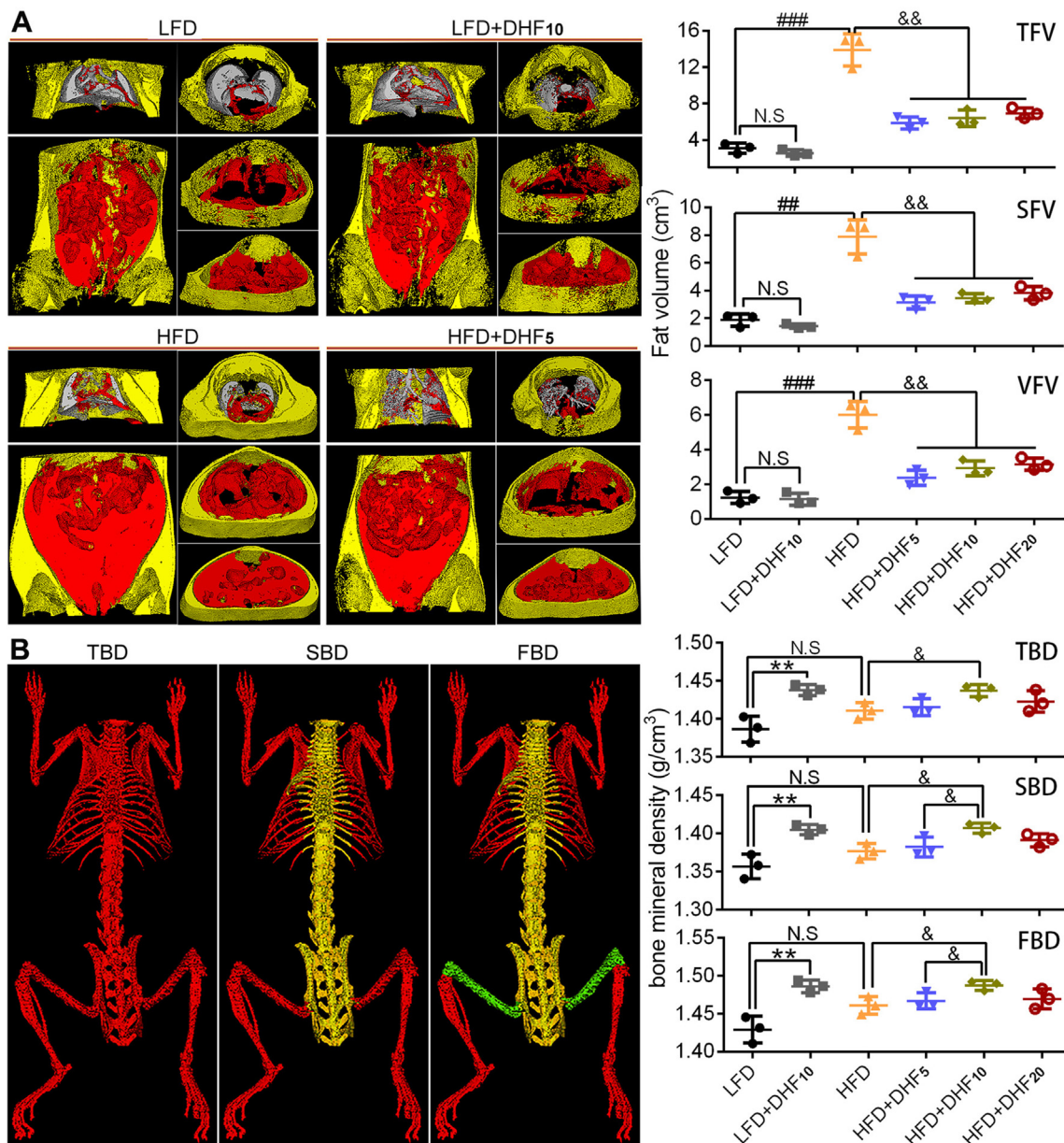
Figure 1: 7,8-DHF reduced diet-induced obesity and increased bone mineral density in mature adult female mice. (A) Quantitative analysis of total fat volume (TFV), subcutaneous fat volume (SFV), and visceral fat volume (VFV) by micro-CT (representative coronal and transverse sections from the same experiment; visceral, red; subcutaneous, yellow). (B) Bone mineral density measured by micro-CT. Scan regions of the total body bone density (TBD) are represented in red, spine bone density (SBD) in yellow, and femoral bone density (FBD) in green (n = 3 mice per group; N.S: not significant, $**p < 0.01$, LFD control vs LFD+DHF$_{10}$, Student's t test; N.S: not significant, $^{##}p < 0.01$, $^{###}p < 0.001$, HFD control vs LFD control, Student's t test; $^{&}p < 0.05$, $^{&&}p < 0.01$, HFD control vs HF+DHF$_{5}$, HFD+DHF$_{10}$, and HFD+DHF$_{20}$, one-way ANOVA).

treated HFD-fed mice compared with those in the HFD controls (Figure 1A). Bone mineral density, including total body bone density (TBD), spine bone density (SBD), and femoral bone density (FBD), were also investigated using micro-CT. 7,8-DHF at the medium dose (10 mg/kg·BW) resulted in a marked increase in bone mineral density irrespective of dietary conditions (Figure 1B). Notably, the results also suggested no apparent impact of the HFD on bone mineral density in comparison with the LFD and HFD controls.

We also compared the preventive effects of low, medium, and high doses of 7,8-DHF against HFD-induced obesity. Seventy-two eight-week-old female mice were fed a control LFD or HFD and treated by gavage with three doses of 7,8-DHF (5, 10, or 20 mg/kg·BW) daily for

up to 24 weeks. The dosage was selected based on previous dose—response studies [36,42,43]. The mice on the HFD gained significantly more weight than the LFD-fed mice from 11 weeks of age onward and became markedly obese by 32 weeks of age. The 7,8-DHF-treated mice under HFD gained weight until 17 weeks of age; however, their weight gain tailed off after 20 weeks of age, especially in the 7,8-DHF low-dose group (Supplemental Figure 2). In contrast, administration of 7,8-DHF did not affect the weight gain of the LFD-fed mice (Supplemental Figure 2). The weights of various organs were also measured after the mice were sacrificed (Supplemental Figure 3). 7,8-DHF treatment of the HFD-fed mice markedly reduced the weight of the liver, spleen, and inguinal white adipose tissues (iWAT) compared with

those of the vehicle-treated HFD mice (Supplemental Figure 3A, C, and D). Although there was no obvious impact on the weights of the kidney, spleen, and iWAT in the LFD-fed mice, the weights of iBAT and the liver in the LFD+DHF$_{10}$ group notably increased after 7,8-DHF treatment (Supplemental Figure 3A and E).

Remarkably, the female mice consuming 7,8-DHF at all three doses displayed reduced body weight gain under HFD (Supplemental Figure 2); however, the effect was not dose-dependent. Unexpectedly, in the low-dose group (5 mg/kg·BW), 7,8-DHF showed the optimal result. The food intake of the mice in each group was also tracked regularly (Supplemental Figure 4A and B). Interestingly, supplementation with 7,8-DHF elevated the total food intake in the LFD-fed mice after 20 weeks of age. In contrast, there were no significant differences among the HFD-fed groups. We also monitored food intake during the last week before sacrifice, and 7,8-DHF significantly enhanced the food intake in the LFD-fed mice ($p < 0.05$), but had no impact among the HFD-fed groups (Supplemental Figure 4C). Thus, long-term treatment with 7,8-DHF in the female mice not only prevented HFD-induced body weight gain and fat accumulation, but also increased bone mineral density, regardless of LFD and HFD conditions.

3.2. 7,8-DHF improved systemic lipid metabolism and glucose homeostasis in the LFD and HFD-fed mice

HFD-elicited obesity is associated with various aberrant metabolic characteristics. We observed that HFD feeding for 24 weeks led to severe lipid deposition in hepatocytes compared with that induced by LFD feeding, and lipid deposition was reduced in all of the 7,8-DHF treatment groups (Supplemental Figure 5A). Surprisingly, the LFD control group also displayed aggregation of small lipid droplets in the liver, which was alleviated in the LFD+DHF$_{10}$ group (Supplemental Figure 5A). In addition, the adipocytes in the 7,8-DHF-treated HFD-fed mice were obviously smaller, especially in the 7,8-DHF low-dose group compared with those in the HFD controls (Supplemental Figure 5B). Hence, 7,8-DHF reduced lipid accumulation in ectopic tissue and abrogated adipocyte hypertrophy. Excessive fat accumulation in obese individuals often causes dyslipidemia. The serum TG, FFA, and T-CHO levels in the HFD control group were significantly increased compared with those in the LFD control group ($p < 0.001$, Supplemental Figure 5C-E). In line with the effects of 7,8-DHF on the body weight of the HFD-fed mice, 7,8-DHF markedly relieved dyslipidemia caused by the HFD. Serum TG, FFA, and T-CHO in the 7,8-DHF-treated HFD-fed mice exhibited a significant decrease compared with those in the HFD controls. Interestingly, the LFD-fed mice treated with 7,8-DHF also showed reduced serum TC, FFA, and T-CHO levels.

Obesity also leads to impaired glucose homeostasis and insulin action [54]. Numerous studies have reported that reduction in body weight in obese subjects improved their insulin response. Therefore, we used GTTs and ITTs to investigate whether 7,8-DHF also affected glucose homeostasis and insulin sensitivity. The results showed that the mice in the HFD control group had a higher level of fasting blood glucose and insulin compared with the mice fed an LFD (Supplemental Figure 5F and G). Furthermore, the glucose and insulin tolerance tests showed that the mice on the HFD developed more severe glucose and insulin resistance (HFD control vs LFD control; Supplemental Figure 5H-K). In comparison with the HFD control group, 7,8-DHF lowered the fasting blood glucose level (Supplemental Figure 5F) and reduced circulating insulin (Supplemental Figure 5G). Although there was no difference in fasting blood glucose with or without 7,8-DHF in the LFD-fed mice, the LFD+DHF$_{10}$ group exhibited significantly ($p < 0.001$) lower insulin levels compared with the control group (Supplemental Figure 5G).

Moreover, the GTT and ITT results showed that the 7,8-DHF-treated mice displayed increased glucose tolerance and decreased insulin resistance in both the LFD- and HFD-fed mice. These mice displayed better glucose clearance in the GTTs (Supplemental Figure 5H, I). Additionally, 7,8-DHF also induced increased glucose reduction after injection with insulin (Supplemental Figure 5J and K), indicating that 7,8-DHF also rescued insulin sensitivity in both the long-term HFD- or LFD-fed female mice.

3.3. 7,8-DHF protected against ovarian failure and alleviated systemic inflammation in mature adult mice

Diminished ovarian reserve is a typical clinical manifestation of perimenopausal transition, which is associated with increases in total body fat and decreases in bone mass, all of which impact the quality of later life [10,11]. To test whether 7,8-DHF could improve the ovarian reserve functions and protect the HPO axis in mature adult female mice, we determined serum and tissue parameters related to the HPO axis functions, including estrus cycles, sex-related serum hormone levels, number of follicles at each stage, and uterus coefficients. The results showed that all of the 7,8-DHF treated groups, whether fed an LFD or HFD, showed regular 4- to 5-day estrus cycles (Table 1): proestrus (cells were almost exclusively oval nucleated epithelial cells, Supplemental Figure 6A), estrus (a large number of cornified squamous epithelial cells, Supplemental Figure 6B), metestrus (fragmented, cornified epithelial cells and leukocytes, Supplemental Figure 6C), and diestrus (a large number of leukocytes, with occasional keratinocytes and epithelial cells, Supplemental Figure 6D). In contrast, the mice in the LFD and HFD control groups exhibited markedly prolonged estrus cycles or disordered estrus cycles: periods of diestrus gradually extended, resulting in a sexual cycle taking 7–8 days or even more than 10 days, and the estrus frequency was significantly reduced (vaginal smear with a large number of leukocytes accounting for the majority of cells). In addition, comparison of the estrus frequency between the LFD control and HFD control groups (Table 1) suggested that there were no obvious associations between the estrus frequency and dietary conditions (either LFD or HFD).

Estrus cyclicity is governed by hormonal regulation and HPO axis feedback mechanisms through E2, FSH, luteinizing hormone (LH), and progesterone (PG) [55]. In females, circulating FSH levels increase while E2 concentrations decrease in response to ovarian failure, as the ability to procreate ceases at menopause. ELISA analysis showed that all of the 7,8-DHF treated groups, whether fed an LFD or HFD, had significantly enhanced serum E2 ($p < 0.001$) and lower FSH levels ($p < 0.001$). In addition, the FSH level in the HFD control group was further increased compared with that in the LFD control group, whereas there was no significant difference in E2 levels (Table 1). As an accurate marker of the ovarian reserve, serum AMH levels were also measured. As expected, 7,8-DHF showed higher AMH levels in all of the treated groups compared with those in the untreated control groups. However, there was no significant difference in AMH levels between the LFD control and HFD control groups. Estrogen deficiency caused by ovarian failure is often accompanied by uterine atrophy; therefore, the uterus indexes of each group were further evaluated. As shown in Table 1, the uterus indexes were significantly decreased by HFD feeding (LFD control vs HFD control, $p < 0.001$). In the LFD-fed mice, 7,8-DHF significantly increased the uterus index compared with that of the control group ($p < 0.05$). While in the HFD-fed groups, only the 7,8-DHF medium-dose group (10 mg/kg·BW) showed a statistical difference ($p < 0.05$) in comparison with that of the control group, although an increase in the uterus index was observed in the mice treated with all three doses.

MOLECULAR
METABOLISM

Table 1 — Serum and tissue parameters related to the hypothalamic-pituitary-ovarian (HPO) axis function in mice after treatment with 7,8-DHF for 24 weeks.

Indexes		LFD-fed mice		HFD-fed mice			
		LFD control	LFD + DHF$_{10}$	HFD control	HFD + DHF$_5$	HFD + DHF$_{10}$	HFD + DHF$_{20}$
Estrus frequency (times/week)		0.88 ± 0.15	$1.56 \pm 0.14^{***}$	$0.81 \pm 0.19^{N.S}$	$1.52 \pm 0.19^{\&\&\&}$	$1.55 \pm 0.12^{\&\&\&}$	$1.48 \pm 0.13^{\&\&\&}$
Serum (n = 10—12)	E2 (pg/mL)	36.00 ± 2.85	$51.31 \pm 9.68^{***}$	$37.53 \pm 4.23^{N.S}$	$56.30 \pm 8.20^{\&\&\&}$	$56.06 \pm 6.61^{\&\&\&}$	$52.36 \pm 7.99^{\&\&\&}$
	FSH (mIU/mL)	12.46 ± 2.13	$6.72 \pm 1.14^{***}$	$15.28 \pm 3.02^{\#}$	$7.79 \pm 1.43^{\&\&\&}$	$7.24 \pm 1.22^{\&\&\&}$	$8.19 \pm 1.52^{\&\&\&}$
	AMH (ng/mL)	3.30 ± 0.60	$4.55 \pm 0.63^{***}$	$2.89 \pm 0.56^{\#}$	$4.49 \pm 0.69^{\&\&\&}$	$4.65 \pm 0.62^{\&\&\&}$	$4.35 \pm 0.68^{\&\&\&}$
Uterus (n = 10—12)	Uterus weight (mg)	64.66 ± 15.71	$79.21 \pm 13.03^{*}$	$79.15 \pm 12.77^{\#}$	82.20 ± 10.62^{N}	87.20 ± 14.46^{N}	82.59 ± 14.13^{N}
	Uterus index (%)	0.32 ± 0.06	$0.38 \pm 0.05^{*}$	$0.23 \pm 0.05^{\#\#\#}$	0.28 ± 0.04^{N}	$0.29 \pm 0.05^{\&}$	0.26 ± 0.04^{N}
Ovary (n = 3—4)	Pr (counts)	286.3 ± 35.2	$685.0 \pm 66.8^{***}$	$76.3 \pm 8.0^{\#\#\#}$	$253.3 \pm 33.2^{\&\&\&}$	—	—
	P (counts)	31.7 ± 2.4	$68.3 \pm 6.2^{**}$	$6.5 \pm 2.1^{\#\#\#}$	$58.3 \pm 14.3^{\&\&\&}$	—	—
	S (counts)	43.7 ± 6.3	$88.7 \pm 5.8^{**}$	$35.5 \pm 7.3^{N.S}$	$96.7 \pm 10.3^{\&\&\&}$	—	—
	A (counts)	46.3 ± 1.9	$52.0 \pm 5.2^{n.s}$	$32.5 \pm 8.3^{\#}$	$88.3 \pm 8.5^{\&\&\&}$	—	—
	Af (counts)	2196.7 ± 248.7	$1293.3 \pm 149.7^{***}$	$2915.5 \pm 309.3^{\#}$	$2076.7 \pm 241.4^{\&}$	—	—

Pr: primordial follicles; P: primary follicles; S: secondary follicles; A: healthy antral follicles; Af: atretic follicles. The uterus index was calculated as uterus weight divided by body weight. N.S: not significant, $*p < 0.05$, $**p < 0.01$, $***p < 0.001$ vs the LFD control group, Student's t test; N: not significant, $\&p < 0.05$, $\&\&\&p < 0.001$ vs the HFD control group, one-way ANOVA; N.S: not significant, $\#p < 0.05$, $\#\#\#p < 0.001$ vs the LFD control group, Student's t test; "—" represents not tested.

As a complementary *in vivo* test of ovarian failure, ovarian morphology was further examined (Figure 2A—D). Each ovarian section was assessed for the number of primordial follicles (Pr) (Figure 2E), primary follicles (P) (Figure 2F), secondary follicles (S) (Figure 2G), antral follicles (A) (Figure 2H), and atretic follicles (Af) (Figure 2I). Notably, 7,8-DHF induced marked changes to the follicles in each stage in both the LFD- and HFD-fed mice (Table 1). Specifically, 7,8-DHF significantly increased the number of Pr, P, and S follicles, accompanied by a significant decline in Af compared with that of the control group. However, a significant improvement of mature antral follicles by 7,8-DHF was observed in the HFD-fed mice, but not in the LFD-fed groups. HFD feeding further aggravated the loss of primordial follicles and primary follicles and facilitated the death or atretic follicles compared with that observed in the LFD group. Thus, quantification of ovarian follicles revealed that 7,8-DHF greatly promoted follicular development and reduced atretic follicles in the ovaries.

Increased inflammation is closely associated with aging-related diseases, including visceral obesity, insulin resistance, and ovarian failure [54—57]. To examine the suppressive effect on inflammation of 7,8-DHF, we investigated representative pro-inflammatory factors, including IL-6 and TNF-α. The circulating LPS was also investigated because it is often used as a biomarker of inflammation resulting from gut microbiota dysbiosis [58]. The results showed that HFD feeding aggravated the production of serum pro-inflammatory factors (IL-6 and TNF-α) in comparison with the LFD-fed (LFD control vs HFD control, Figure 2J,K). As expected, the HFD induced pro-inflammatory factors IL-6 and TNF-α, and their levels were significantly downregulated by 7,8-DHF at all three doses (Figure 2J,K). Interestingly, 7,8-DHF also markedly suppressed IL-6 and TNF-α levels in the LFD-fed mice. Circulating LPS was also notably downregulated in both the LFD- and HFD-fed groups by 7,8-DHF, indicating that 7,8-DHF might exert a therapeutic effect on gut microbiota homeostasis (Figure 2L).

3.4. 7,8-DHF induced increased ERα gene and protein expression in skeletal muscle

To determine the role of ERα and ERβ in the regulation by 7,8-DHF of MetS in the female mice, we first quantified ERα and ERβ gene expression (*Esr1* and *Esr2*) in skeletal muscle (a mixture of the soleus and gastrocnemius muscles) and adipose tissue (gonadal WAT, gWAT). As shown in Figure 3A, muscle *Esr1* expression levels were markedly elevated by 2.5, 4.1, 4.4, and 4.6 times in the 7,8-DHF-treated groups

(LFD+DHF$_{10}$, HFD+DHF$_5$, HFD+DHF$_{10}$, and HFD+DHF$_{20}$, respectively) compared with that in their corresponding control groups (LFD and HFD control groups). Unexpectedly, however, the Esr1 expression levels in the muscle obviously ($p < 0.01$) increased in the HFD control group compared with the LFD control group (Figure 3A), and the reason for this was not completely clear. Conversely, *Esr1* expression levels in the adipose tissue significantly decreased in the HFD-fed mice compared with those in the LFD-fed mice (HFD control vs LFD control, $p < 0.001$, Figure 3B). Moreover, *Esr1* expression in the adipose tissue only showed a significant increase ($p < 0.001$) in the HFD-fed mice treated with 7,8-DHF compared with that in the HFD control group, whereas there was no significant difference between the LFD+DHF$_{10}$ group and LFD control group (Figure 3B). Compared with *Esr1*, the expression of *Esr2* was more complicated. Muscle *Esr2* expression levels were notably increased in a dose-dependent manner by 7,8-DHF in the HFD-fed mice; however, its expression was prominently down-regulated by nearly 50% ($p < 0.01$) in the LFD+DHF$_{10}$ group compared with that in the LFD control group (Figure 3C). In contrast, markedly enhanced expression of *Esr2* in the adipose tissue in both the LFD- and HFD-fed groups was observed upon 7,8-DHF treatment (Figure 3D).

We then assessed the protein levels of ERα in skeletal muscle and visceral white adipose tissue using immunoblotting and found that 7,8-DHF induced significantly upregulated levels of ERα in muscle (Figure 3E, third panel), whereas upregulation of ERα in adipose tissue was only observed in the 7,8-DHF treated HFD-fed mice (Figure 3F, third panel). Thus, the trend in ERα protein levels was consistent with the mRNA levels. Additionally, the levels of the two main phosphorylated forms of the ERα protein (phosphorylated at serine 118 (S188) and tyrosine 537 (Y537) sites located in the activation function-1 (AF-1) domain and activation function-2 (AF-2) domain, respectively) were both elevated by 7,8-DHF in skeletal muscle (Figure 3E, first and second panels).

As expected, 7,8-DHF triggered TrkB phosphorylation in skeletal muscle (Figure 3E, fourth panel), but not in adipose tissue (Figure 3F, fourth panel), which was in line with previous reports [42]. Downstream AKT phosphorylation was evidently increased in muscle in the LFD- and HFD-fed mice by 7,8-DHF. Surprisingly, AKT phosphorylation was also observed in the adipose tissues of the 7,8-DHF-treated HFD-fed mice in the absence of TrkB activation, which might have been attributed to the enhanced levels of ERα and its phosphorylated forms. In agreement with these results, the levels of uncoupling protein 1 (UCP1), a mitochondrial protein that is responsible for non-shivering thermogenesis in brown
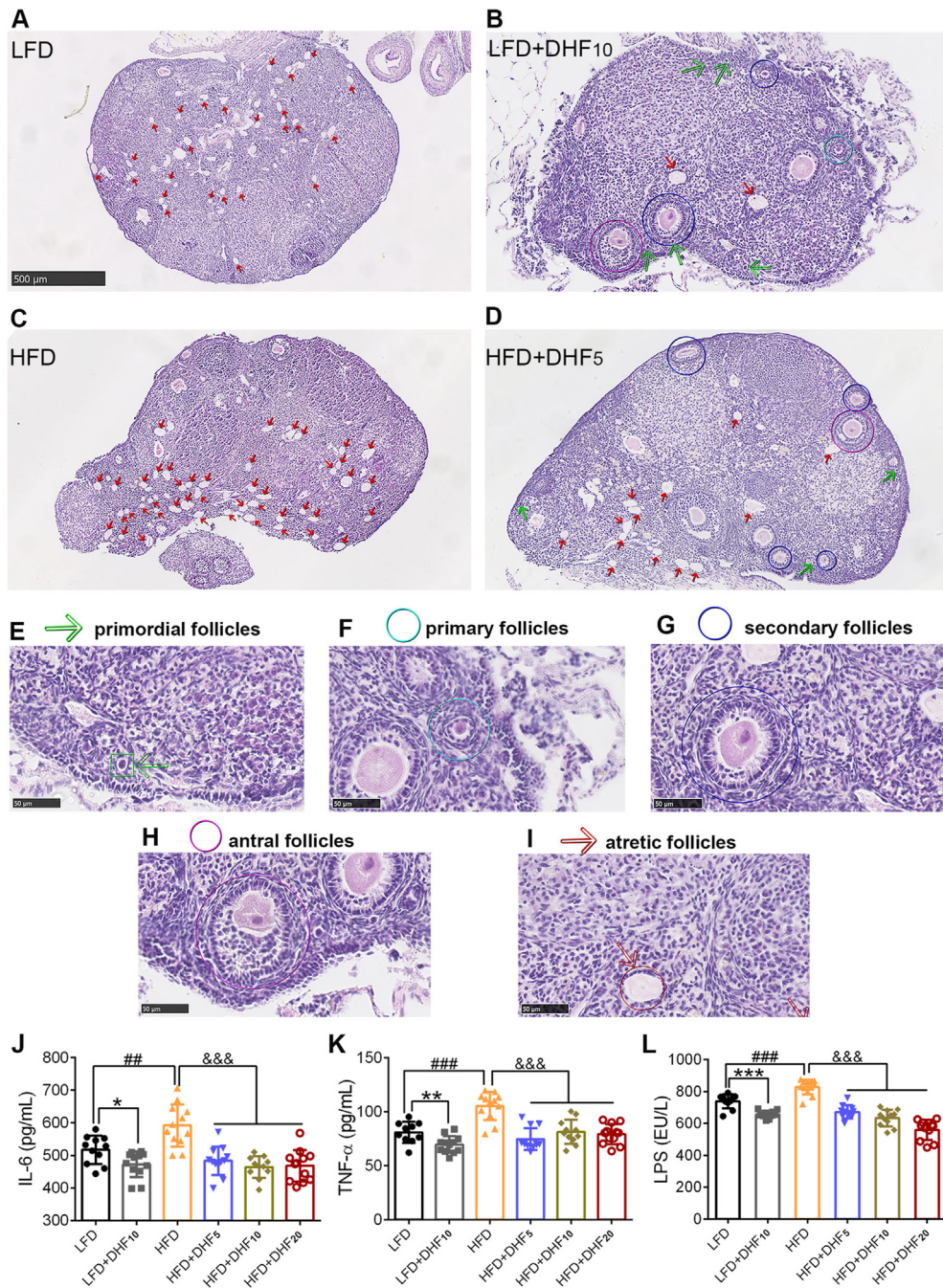
Figure 2: 7,8-DHF protected against ovarian failure and alleviated inflammation in mature adult female mice. Representative ovarian sections that were stained with H-E to visualize morphological structures in **(A)** LFD control group, **(B)** LFD+DHF$_{10}$ group, **(C)** HFD control group, and **(D)** HFD+DHF$_5$ group (n = 3−4 per group, scale bars 500 μm). Follicles were counted and classified as primordial follicles as shown in **(E)** and indicated with green arrows; primary follicles as shown in **(F)** and marked by cyan circles; secondary follicles as shown in **(G)** and indicated with blue circles; healthy antral follicles as shown in **(H)** and indicated with purple circles; and atretic follicles as shown in (I) and indicated with red arrows. The classification method for different stage follicles was performed mainly according to previous reports [56,57]. **(J)−(L)** Serum concentrations of IL-6, TNF-α, and LPS (n = 10−12; $*p < 0.05$, $**p < 0.01$, $***p < 0.001$, LFD control vs LFD+DHF$_{10}$, Student's t test; $^{##}p < 0.01$, $^{###}p < 0.001$, HFD control vs LFD control, Student's t test; $^{\&\&\&}p < 0.001$, HFD control vs HFD+DHF$_5$, HF+DHF$_{10}$, and HFD+DHF$_{20}$, one-way ANOVA).

adipose tissue (BAT) [59], were also specifically induced in the skeletal muscle of the 7,8-DHF-treated mice, regardless of LFD or HFD feeding (Figure 3E, eighth panel), but not in adipose tissue (Figure 3F, eighth panel). Taken together, these results suggested that the activation of TrkB combined with ERα acted together to regulate the effect of 7,8-DHF on MetS. Thus, we next focused on the mechanism of the mutual regulation between TrkB and ERα in the energy metabolism in skeletal muscle.

3.5. 7,8-DHF stimulated glucose consumption in an ERα- or TrkB-dependent manner

7,8-DHF directly stimulated glucose consumption in a dose-dependent manner in C2C12 myotubes, and the glucose consumption in the 7,8-DHF high-dose group (5 μmol/L) increased by nearly two-fold compared with that of the control group (Figure 4A). As a control, BDNF also elevated glucose consumption; however, this was
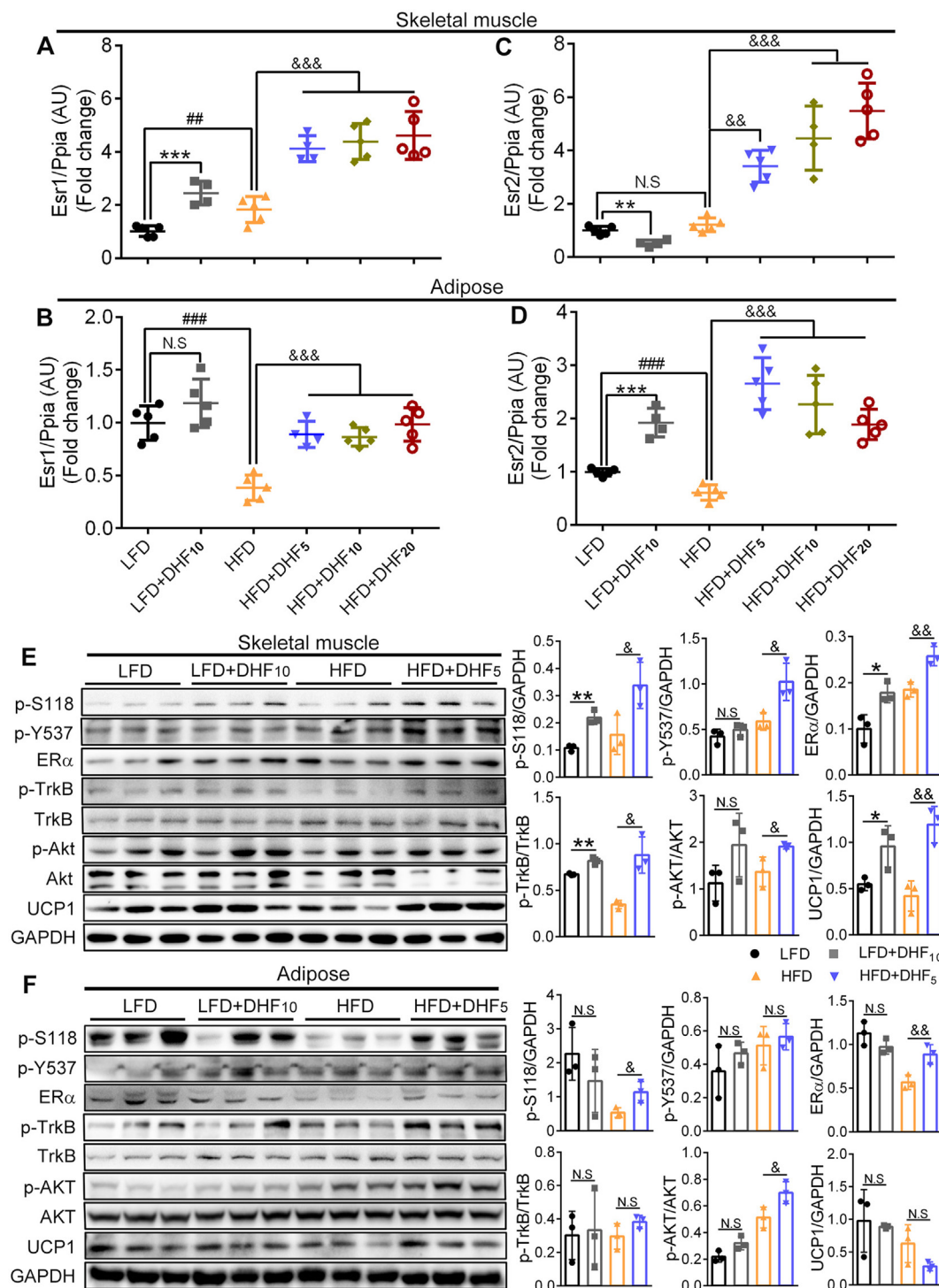
Figure 3: Effect of 7,8-DHF treatment on gene and protein levels of ERα and ERβ in skeletal muscle and adipose tissues. (A)−(D) ERα gene (*Esr1*) and ERβ gene (*Esr2*) levels in skeletal muscle and adipose tissues. The skeletal muscles were isolated from mouse thigh, which contained mixed muscle fiber types, while adiposes used were the visceral WAT ($n = 4$−5, $**p < 0.01$, $***p < 0.001$, N.S: not significant, LFD control vs LFD+DHF$_{10}$, Student's t test; $^{##}p < 0.01$, $^{###}p < 0.001$, N.S: not significant, HFD control vs LFD control, Student's t test; $^{&&}p < 0.01$, $^{&&&}p < 0.001$, HFD control vs HFD+DHF$_5$, HFD+DHF$_{10}$, and HFD+DHF$_{20}$, one-way ANOVA). (E)−(F) Western blotting analysis of skeletal muscle and adipose tissues isolated from mice that were treated with 7,8-DHF for 24 weeks. Protein levels of ERα and its two phosphorylated forms p-S118 and p-Y537, the phosphorylation of TrkB, and two key energy metabolism-related proteins AKT and UCP1 were measured. Representative immunoblots and quantification are shown ($n = 3$ per group. $*p < 0.05$, $**p < 0.01$, N.S: not significant, LFD control vs LFD+DHF$_{10}$, Student's t test; $^{&}p < 0.05$, $^{&&}p < 0.01$, N.S: not significant, HFD control vs HFD+DHF$_5$, Student's t test).

significant only for the high-dose group (200 ng/mL) ($p < 0.05$) in comparison with the corresponding control group (Figure 4B).

To investigate the role of ERα and TrkB in 7,8-DHF-mediated muscular glucose consumption in a muscle cell line, we employed specific blockers of ERα and TrkB, ICI182780, and k252a, respectively. The promoting effects of 7,8-DHF or BDNF on glucose consumption was abolished using either the ERα antagonist (ICI18278) or TrkB inhibitor (k252a) (Figure 4A,B).

3.6. The mechanism of ERα activation by 7,8-DHF

To investigate the mechanism by which 7,8-DHF modulates ERα, we first compared the effect of 7,8-DHF/BDNF on the activation of several relevant signaling pathways in C2C12 myotubes in the presence of the specific TrkB inhibitor (k252a). The TrkB receptor was gradually activated by 7,8-DHF or BDNF in a time-dependent manner and this

activation was blocked by k252a (first panel in Figure 5A; Figure 5B). Interestingly, activation of ERα at the Y537 site was markedly suppressed by k252a (fourth panel in Figure 5A; Figure 5C). However, k252a alone substantially augmented the level of phosphorylated ERα S118 (p-S118) and failed to block 7,8-DHF or BDNF-induced p-S118 signals (third panel in Figure 5A; Figure 5D). Similar to previous findings, 7,8-DHF or BDNF induced activation of the TrkB signaling pathway, in which AKT phosphorylation (tenth panel in Figure 5A; Figure 5E) and the UCP1 level (twelfth panel in Figure 5A; Figure 5F) increased in a time-dependent manner and were then suppressed by k252a.

Insight into the kinases required for 7,8-DHF-induced phosphorylation of ERα is critical to understand the signaling mechanisms by which ERα is transactivated by 7,8-DHF. Thus, the phosphorylation of MAPK-ERK1/2 (ERK) and proto-oncogene, non-receptor tyrosine kinase (Src) were tested because they have been verified as the two main kinases
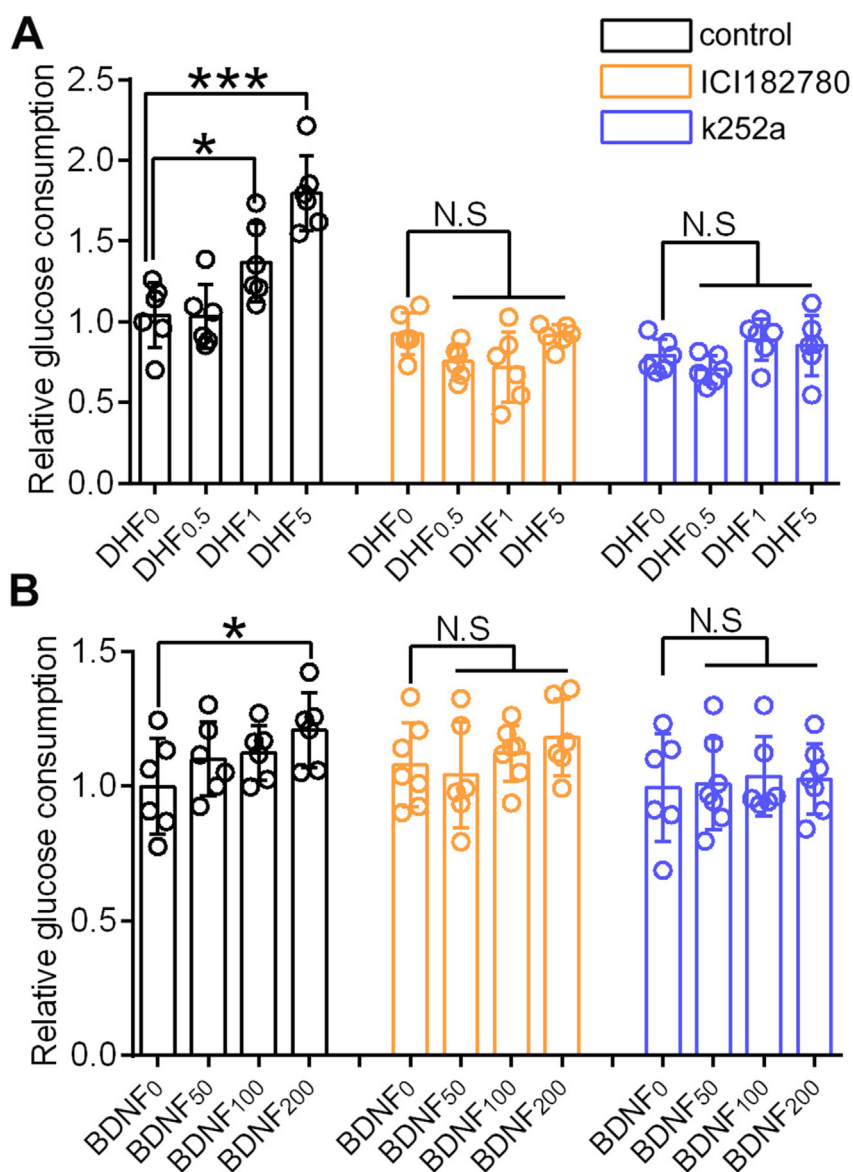
Figure 4: The promotion effects of 7,8-DHF or BDNF on glucose consumption in C2C12 myotubes could be abolished by ERα or TrkB inhibitors. (A) Differentiated C2C12 myotubes were incubated with low, medium, and high concentrations of 7,8-DHF (0.5, 1, and 5 μmol/L, respectively), or **(B)** BDNF (50, 100, and 200 ng/mL, respectively) for 16 h with or without ICI182780 or k252a. Myotubes were preincubated with ICI182780 (1 μmol/L) or k252a (30 nmol/L) for 1 h (n = 6−7, *$p < 0.05$, ***$p < 0.001$, N.S: not significant, one-way ANOVA).

Figure 5: 7,8-DHF transactivated ERα by activating its corresponding kinases ERK and Src. (A) Specific TrkB inhibitor, k252a, inhibited 7,8-DHF- or BDNF-induced phosphorylation of ERα at tyrosine 537 (p-Y537) but not at serine 118 (p-S118). Differentiated C2C12 myotubes were incubated with TrkB kinase inhibitor k252a (30 nmol/L) or vehicle for 1 h followed by BDNF (100 ng/mL) for 10 min, 1 h or 7,8-DHF (1 μmol/L) for 10 min, 1 h, or 6 h. Cell lysates were then collected and the phosphorylation of TrkB (first panel), ERα (third and fourth panels), ERK (sixth panel), Src (eighth panel), and AKT (tenth panel) was examined. Total TrkB (second panel), ERα (fifth panel), ERK (seventh panel), Src (ninth panel), AKT (eleventh panel), UCP1 (twelfth panel), and tubulin (thirteenth panel) were also verified. (B)—(H) Densitometric measurements of bands in (A) were performed, and the expression levels of target proteins in the control group (con, without k252a) were normalized to 1. Representative images and densitometries from three independent experiments are shown (n = 3, N.S: not significant, $*p < 0.05$, $**p < 0.01$, $***p < 0.001$, Student's t test; N.S: not significant, $^{\&}p < 0.05$, $^{\&\&}p < 0.01$, $^{\&\&\&}p < 0.001$, vs control group without k252a, one-way ANOVA). (I) Inhibition of ERK abolished 7,8-DHF or BDNF-induced phosphorylation of S118 and the activation of Src. Differentiated C2C12 myotubes were preincubated with SCH772984 (1 μmol/L) or vehicle for 1 h followed by BDNF (100 ng/mL) or 7,8-DHF (1 μmol/L) for various time intervals as indicated. Cell lysates were then collected and the phosphorylation of ERK (first panel), ERα at the S118 site (third panel), and Src (fifth panel) was examined by immunoblotting. Total ERK (second panel), ERα (fourth panel), and Src (sixth panel) were also verified. (J) Inhibition of Src diminished 7,8-DHF or BDNF-induced TrkB activation and p-Y537. Differentiated C2C12 myotubes were preincubated with PP1 (5 μmol/L) or vehicle for 1 h followed by BDNF (100 ng/mL) or 7,8-DHF (1 μmol/L) for various time intervals as indicated. Cell lysates were then collected and the phosphorylation of Src (first panel), TrkB (third panel), and ERα Y537 (fifth panel) was measured. Total Src (second panel), TrkB (fourth panel), and ERα (sixth panel) were also verified.

responsible the activation of ERα at S118 and Y537, respectively [60]. As expected, phosphorylated (p)-ERK was distinctly enhanced by treatment with 7,8-DHF or BDNF compared with that in the control group, especially at the 10 min time point. k252a further elevated p-ERK, which was consistent with the trend in ERα S118 activation (sixth panel in Figure 5A; Figure 5G). Notably, 7,8-DHF- or BDNF-induced p-Src correlated with the activation of ERα Y537 (eighth panel in Figure 5A; Figure 5H). These findings suggested that 7,8-DHF-induced phosphorylation of ERα at S118 and Y537 was partly achieved by activating their corresponding kinases, ERK and Src, which might in turn depend on activation of the BDNF/TrkB signaling pathway. Subsequently, we tested this hypothesis using two specific small molecule inhibitors of ERK and Src. As shown in Figure 5I, the ERK inhibitor

SCH772984 inhibited 7,8-DHF-induced phosphorylation of ERα at S118, and phosphorylation of Src was also suppressed by SCH772984, which might be attributed to the inactivation of ERα S118 phosphorylation [61]. As expected, inhibiting Src using its specific inhibitor PP1 suppressed p-ERα at Y537 (Figure 5J). Remarkably, 7,8-DHF- or BDNF-induced phosphorylation of TrkB was also blocked by the Src inhibitor (Figure 5J).

3.7. ERα deletion impaired the activation of TrkB and its downstream energy metabolism-related signaling molecules
To further determine the mechanism involved in the interplay between ERα and TrkB receptors in 7,8-DHF-induced metabolic improvement, a small molecule ERα antagonist ICI182780 and short hairpin RNA

(shRNA)-mediated knockdown of *Esr1* were successively employed to deplete ERα in C2C12 myotubes. As shown in Figure 6A,B, incubation with ICI182780 (5 μmol/L) for 6 h induced a significant degradation of ERα in differentiated C2C12 myotubes, which was consistent with the results of a previous report [62]. Interestingly, with the suppression of ERα, 7,8-DHF- or BDNF-induced phosphorylation of TrkB (Figure 6A,C), as well as its downstream signaling molecules, including Src (Figure 6A,D), AKT (Figure 6A,E), and UCP1 (Figure 6A,F), were all inhibited. However, p-ERK was not affected (Figure 6A,G), implying that ERK might act upstream of ERα in this setting.

We then used a lentivirus-shRNA strategy to knockdown *Esr1* in C2C12 myoblasts to further confirm these results. Three different *Esr1*-targeting shRNA sequences (Esr1-KD1, Esr1-KD2, and Esr1-KD3) were tested and resulted in 62, 74, and 26% reductions, respectively, of *Esr1* expression (Figure 6H as quantified using quantitative real-time reverse transcription PCR (qRT-PCR)) and 48, 60, and 28% reductions, respectively, in the ERα protein level (Figure 6I,J as quantified using Western blotting). Thus, Esr1-KD2 was selected for subsequent study because of its outstanding silencing efficiency on *Esr1*. As shown in Figure 6K, *Esr1* knockdown markedly impaired TrkB
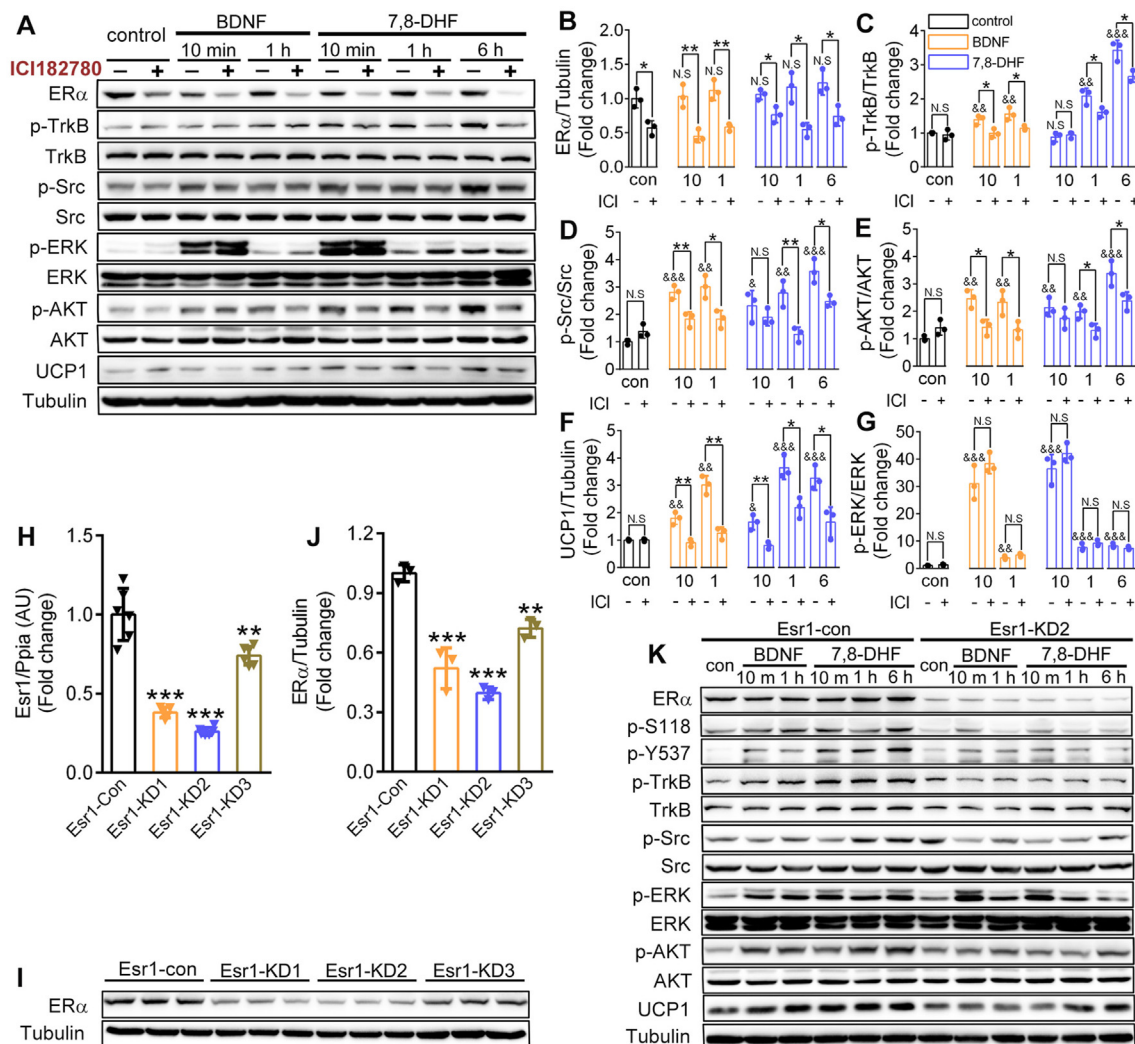
Figure 6: Deletion of ERα impaired 7,8-DHF-stimulated activation of BDNF/TrkB signaling cascades. (A) Inhibition of ERα by ICI182780 suppressed 7,8-DHF- or BDNF-induced TrkB activation. Differentiated C2C12 myotubes were preincubated with ICI182780 (5 μmol/L) or vehicle for 6 h and then continued for various time intervals as indicated in the presence of vehicle, BDNF (100 ng/mL), or 7,8-DHF (1 μmol/L). Cell lysates were then collected and the phosphorylation of TrkB (second panel), Src (fourth panel), ERK (sixth panel), and AKT (eighth panel) was examined by immunoblotting. Total ERα (first panel), TrkB (third panel), Src (fifth panel), ERK (seventh panel), AKT (ninth panel), and the expression of UCP1 (tenth panel) and tubulin (eleventh panel) were also verified. **(B)−(G)** The densitometric measurements of protein bands in **(A)** and the expression levels of target proteins in the control group (con, without ICI182780, abbreviated as ICI) were normalized to 1. Representative images and densitometries from three independent experiments are shown (n = 3, N.S: not significant, $*p < 0.05$, $**p < 0.01$, Student's t test; N.S: not significant, $^{\&\&}p < 0.01$, $^{\&\&\&}p < 0.001$, vs the control group without ICI182780, one-way ANOVA). **(H)−(J)** ERα gene (*Esr1*) expressions **(H)**, ERα protein levels **(I)**, and densitometric measurements of ERα protein levels relative to tubulin expression **(J)**. Esr1-KD achieved by lentiviral delivery of short hairpin RNA (one control and three clones tested and marked as Esr1-con, Esr1-KD1, Esr1-KD2, and Esr1-KD3). Densitometric analyses are expressed as means ± SD in arbitrary units normalized to 1.0. n = 5−6 for *Esr1* qRT-PCR test in **(H)**; n = 3 for ERα immunoblotting in **(I)** and **(J)**. $**p < 0.01$, $***p < 0.001$ vs control group, one-way ANOVA. **(K)** Esr1-KD impaired 7,8-DHF-stimulated BDNF/TrkB-signaling cascades in C2C12 myotubes. Differentiated control (Esr1-con) or Esr1-KD2 C2C12 myotubes were incubated in BDNF (100 ng/mL) or 7,8-DHF (1 μmol/L) for various time intervals as indicated. Cell lysates were then collected and the phosphorylation of ERα at the S118 (second panel) and Y537 (third panel) sites, TrkB (fourth panel), Src (sixth panel), ERK (eighth panel), and AKT (tenth panel) was examined. Total ERα (first panel), TrkB (fifth panel), Src (seventh panel), ERK (ninth panel), AKT (eleventh panel), and the expression of UCP1 (twelfth panel) and tubulin (thirteenth panel) were also verified. Control is abbreviated as con.

signal transduction as evidenced by the observations that 7,8-DHF or BDNF-stimulated phosphorylation of TrkB, Src, AKT, and UCP1 expression were all markedly reduced compared with those in the scramble shRNA group (Esr1-con group).

4. DISCUSSION

Previous studies [42,43] indicated that 7,8-DHF-stimulated activation of muscular TrkB alleviated HFD-induced obesity of female mice in a sex-specific manner. However, the underlying molecular mechanism for this sex-related dimorphism is unknown. In this study, we revealed a key functional activity of 7,8-DHF in activating ERα in skeletal muscle, which is essential for the activation of muscular TrkB and its downstream energy metabolism-related signaling cascades. *In vivo* animal experiments suggested that long-term intake of 7,8-DHF exerted a significant regulatory role on the HPO axis in mice as evidenced by its protective effect on ovarian reserve function and the maintenance of the homoeostasis of HPO axis-regulated sex hormones (represented by E2 and FSH). Consequently, 7,8-DHF treatment not only resulted in increased bone mass, but also a marked reduction in adiposity and its complications coupled with the production of ERα protein-rich, TrkB-activated, and UCP1-high thermogenic skeletal muscle tissue. The *in vitro* cellular experiments further revealed the specific signaling pathways involved in the interplay of ERα and TrkB receptors, indicating that ERα in C2C12 myotubes is crucial for the 7,8-DHF-activated BDNF/TrkB signaling pathway, which plays an important role in muscle energy metabolism. To the best of our knowledge, this is the first study to investigate the HPO axis-regulated sex hormone levels and functional hormone receptor ERα alteration by 7,8-DHF and discover the sex differences in 7,8-DHF-induced prevention of MetS.

After women enter menopause, poor ovarian reserve, combined with reduced estrogen and increased FSH, lead to postmenopausal obesity, osteoporosis, and perimenopausal syndrome [11,63]. The reduced estrogen action has been clinically associated with obesity, metabolic dysfunction, and increased risk of chronic disease [20]. Based on these facts, we suspected that the sex-specific hormones and their receptors would dominate the sex-dependent anti-metabolic syndrome activity of 7,8-DHF in female mice. To test this idea, both LFD- and HFD-fed C57BL/6J female mice were subjected to long-term administration by gavage, with or without 7,8-DHF, until significant estrus frequency changes were detected. The results indicated that long-term 7,8-DHF administration effectively alleviated HFD-induced obesity and corresponding metabolism dysfunction, including hyperlipidemia, hyperinsulinemia, fat accumulation in the liver, and bone loss. Although there was no significant difference in body weight changes observed between the 7,8-DHF intervention and LFD control groups, prominent improvement of glucose tolerance, insulin sensitivity, and bone mineral density was observed in the LFD+DHF$_{10}$ group of mice, suggesting that 7,8-DHF also plays a regulatory role in metabolism dysfunction, even in LFD-fed mice.

As expected, long-term intervention with 7,8-DHF exhibited a profound protective effect on the functions of the HPO axis, protecting against ovarian aging and earlier menopause in the mature adult female mice. As shown in Table 1, both the LFD and HFD control groups (without treatment with 7,8-DHF) exhibited a prolonged estrus frequency, elevated FSH, and reduced E2, AMH, and uterus index. In addition, follicle counts suggested that healthy oocyte development caused severe injury in the mice in the absence of 7,8-DHF, especially in the HFD control group (Table 1). In general, the C57BL/6J strain of mouse enters the perimenopausal stage at 10—14 months old [64].

However, the mice in the LFD and HFD control groups showed marked perimenopausal symptoms at only 8 months of age, which was further accentuated after HFD feeding. We speculated that this earlier perimenopausal entry was partially related to the stress response caused by long-term daily oral gavage, which undoubtedly induced stress responses and thus interfered with endocrine responses [65,66]. Thus, caution should be employed when selecting the administration methods, and intra-gastric gavage should be avoided when possible.

Moreover, while the specific mechanism by which 7,8-DHF contributes to the protection from ovarian aging and earlier perimenopause onset is not clear; however, based on our current results, it could be speculated that at least two factors are responsible for the benefits. The first is alleviation of systemic inflammation. It is widely accepted that chronic inflammation is one of the characteristics of senescence and aging [55,56,67]. Previous studies have shown that increases in pro-inflammatory cytokines, including IL-6, TNF-α, and IL-1, are closely associated with the decline in ovarian function and estrogen with menopause [68,69]. Inflammation is also involved in the pathogenesis of obesity, T2D, and menopause-associated bone loss, three conditions that contribute to and correlate with aging in the human population [55,69]. Hence, 7,8-DHF-induced amelioration of ovarian failure and metabolic disorders in stressed female mice might function partially through its anti-inflammatory efficacy. The second presumably is via regulation of the gut microbiota. To date, considerable research has been devoted to investigating the gut—brain axis, with a steadily growing appreciation of the gut microbiota, which might contribute to aging and influence CNS function in health and disease [70,71]. Our recent research proved that R13, a prodrug of 7,8-DHF, acted as a prebiotic in the gut and decreased gut leakage and oxidative stress in Alzheimer's disease (AD) model mice, alleviating gut dysbiosis and AD [71]. The circulating endotoxin LPS, which is derived from the release of some Gram-negative bacteria in the intestines, was notably reduced by treatment with 7,8-DHF. LPS has been widely recognized as one of the early trigger factors of low-grade inflammation [72,73] and could be released from gut microbiota into the bloodstream through impaired intestinal integrity induced by gut dysbiosis [74,75]. In turn, an influx of LPS activates Toll-like receptor 4 (TLR4)-dependent signaling, leading to inflammation, which aggravates obesity and insulin resistance [4,75,76]. In short, reduced LPS induced by the intake of 7,8-DHF likely replaced the imbalanced gut flora caused by HFD or other factors and in turn modulated the function of the HPO axis function via the gut—brain axis [77].

Paralleling earlier perimenopause onset and severe metabolic syndrome in the LFD and HFD control group mice, there was a marked reduction in muscle ERα protein accompanied by inactivation of BDNF/TrkB signaling cascades. A large body of evidence shows that skeletal muscle ERα plays a critical and protective role in regulating metabolic homeostasis and insulin sensitivity through multiple pathways, such as maintenance of mitochondrial function and promoting the membrane-trafficking activity of insulin-responsive glucose transporter type 4 (GLUT4) [19,20,78]. Moreover, the occurrence of MetS in perimenopausal women and animals is often accompanied by reduced muscle ERα levels [19]. Subsequently, we examined whether ERα signaling is directly involved in 7,8-DHF-stimulated glucose consumption in C2C12 myotubes. Our findings suggested that 7,8-DHF clearly increased cellular glucose consumption in a dose-dependent manner; however, these effects were abolished by the ERα antagonist ICI182780, which was similar to treatment with the TrkB inhibitor k252a. The same trend was also found in the BDNF control groups. Therefore, it seems plausible that variation in ERα in muscle has an important function in

7,8-DHF-induced improvement of energy metabolism. Again, considering that the promoting effect of 7,8-DHF on skeletal muscle energy consumption is primarily mediated through activation of BDNF/TrkB signaling cascades [42,43], this raises the question as to the possible molecular mechanisms involved in the interplay of ERα and BDNF/TrkB signaling.

ERα is a modular protein consisting of a number of functional domains, including an N-terminal domain, two transcriptional activation functions (AF-1 and AF-2), a centrally located DNA binding domain, a hinge region, and a C-terminal ligand-binding domain [60]. In the classical genomic pathway, ERα function is strongly activated by binding to the estrogen ligand, and then receptors dimerize and bind to specific sequence motifs called estrogen response elements [19,79]. However, more recent studies have shown that ERα function could also be regulated by posttranslational modifications, most significantly by phosphorylation [60]. Most ERα phosphorylation sites are located in the N-terminal domain and are regulated by ligand binding and ligand-independent mechanisms such as peptide growth factor signaling [60,80,81]. ERα regulates transcription through its two activation domains, AF-1 and AF-2. S118 is the most well-characterized phosphorylation site of ERα in AF-1, while as a rare tyrosine phosphorylation site, Y537, is responsible for the activation of the AF-2 domain [60,82]. The present study showed that both S118 and Y537 could be effectively activated by 7,8-DHF or BDNF in C2C12 myotubes without changing the total ERα levels, which was quite different from the results in vivo. We speculated that increased ERα in mouse skeletal muscle was presumably acquired as an indirect effect of 7,8-DHF treatment, such as protecting against ovarian aging and delaying perimenopause onset [19]. Using small molecule inhibitors (SCH772984 and PP1), we confirmed that phosphorylation of ERα at S118 and Y537 was achieved by activating their corresponding kinases, ERK and Src, respectively [82—86]. ERK and Src signaling pathways are also involved in BDNF/TrkB signaling cascades. ERK could be robustly activated through BDNF- or 7,8-DHF-induced activation of TrkB, which is necessary to promote skeletal muscle energy consumption or protect neuronal survival [34,42,43]. Huang et al. reported that TrkB activation by BDNF was capable of promoting Src family kinase activity [87]. Moreover, our results showed that inhibiting the kinase activity of TrkB using the specific inhibitor k252a diminished BDNF- or 7,8-DHF-induced ERα phosphorylation at Y537, but not S118, which might be attributed to the abnormal activation of ERK by k252a. As shown in Figure 5A, k252a enhanced the p-ERK level regardless of the inhibition of TrkB. This unexpected result indicated that ERK could also be activated by k252a, possibly through other signaling pathways, rather than by BDNF/TrkB signaling. Considering these findings, we suggest that activation of ERα S118 is not the decisive factor for 7,8-DHF-stimulated glucose consumption in C2C12 myotubes. Taken together, it is logical to deduce that signaling through growth factors might enhance the activity of ERα via 7,8-DHF-stimulated phosphorylation of ERα at the S118 and Y537 residues within the transactivating domain of ERα.

To further investigate the role of ERα in the activation of 7,8-DHF-induced BDNF/TrkB signaling cascades, we silenced ERα using antagonist ICI182780 and an shRNA. Both strategies indicated that ERα deficiency markedly diminished BDNF- or 7,8-DHF-induced activation of BDNF/TrkB signaling cascades, including phosphorylation of Src and AKT and the expression of UCP1. Surprisingly, robust phosphorylation of ERK stimulated by BDNF or 7,8-DHF at 10 min was not attenuated by deletion of ERα, implying that ERK lies upstream of ERα in this setting. More importantly, we found

that the Src family kinases played a central role in the mutual regulation of ERα and neurotrophin receptor TrkB, which can be explained as follows: First, inhibition of Src activity resulted in the diminished phosphorylation of TrkB and Y537 stimulated by 7,8-DHF simultaneously (Figure 5J); second, inactivation of ERα S118 caused by ERK inhibitor SCH772984 was also paralleled by attenuated Src phosphorylation (Figure 5I); third, inactivation of TrkB by its specific inhibitor k252a blocked 7,8-DHF-induced p-Src and thus weakened p-ERα Y537 (Figure 5A,C, and H); and fourth, silencing ERα could also inhibit the activation of TrkB and Src (Figure 6A,K). A previous study showed that Src family kinases act both downstream and upstream of BDNF-mediated TrkB activation, and Src provides positive feedback regulation of TrkB signaling induced by BDNF [87].

In conclusion, 7,8-DHF, a BDNF mimetic small molecule compound, by protecting against inflammation-induced ovarian failure in stressed female mice and maintaining the role of muscular ERα, has critical effects on improving muscular energy consumption and systematic metabolic homeostasis. This research provides solid evidence that 7,8-DHF-induced activations of ERα and TrkB are interdependent, working synergistically to activate signaling pathways related to energy metabolism, including ERK, AKT, and UCP1. Moreover, as a protective factor that prevents the onset of earlier menopause, 7,8-DHF probably alleviates MetS by decreasing age-relevant accrual of visceral fat and pro-inflammatory cytokines. In turn, 7,8-DHF-induced improvements of these age-associated alterations in metabolism and body fat accumulation are active participants in a virtuous cycle that could prevent the aging process and the onset of metabolic diseases. Collectively, the current findings clearly imply that the maintenance or activation of ERα in muscle would be of therapeutic benefit to treat women with metabolic diseases. Our findings also provide a potential explanation for the sex differences in the 7,8-DHF-mediated alleviation of MetS.

DATA AVAILABILITY

All of the source data are available from the corresponding authors upon reasonable request.

AUTHOR CONTRIBUTIONS

ACKNOWLEDGMENTS

REFERENCES

[1] Cornier, M.A., Dabela, D., Hernandez, T.L., Lindstrom, R.C., Steig, A.J., Stob, N.R., et al., 2008. The metabolic syndrome. Endocrine Reviews 29(7): 777—822.

[2] Hinnouho, G.M., Czernichow, S., Dugravot, A., Nabi, H., Brunner, E.J., Kivimaki, M., et al., 2015. Metabolically healthy obesity and the risk of cardiovascular disease and type 2 diabetes: the Whitehall II cohort study. European Heart Journal 36(9):551—559.

[3] Kaliannan, K., Robertson, R.C., Murphy, K., Stanton, C., Kang, C., Wang, B., et al., 2018. Estrogen-mediated gut microbiome alterations influence sexual dimorphism in metabolic syndrome in mice. Microbiome 6(1):205.

[4] Zhuang, P., Shou, Q., Lu, Y., Wang, G., Qiu, J., Wang, J., et al., 2017. Arachidonic acid sex-dependently affects obesity through linking gut microbiota-driven inflammation to hypothalamus-adipose-liver axis. Biochimica et Biophysica Acta - Molecular Basis of Disease 1863(11):2715—2726.

[5] Franconi, F., Seghieri, G., Canu, S., Straface, E., Campesi, I., Malorni, W., 2008. Are the available experimental models of type 2 diabetes appropriate for a gender perspective? Pharmacological Research 57(1):6—18.

[6] Hwang, L.L., Wang, C.H., Li, T.L., Chang, S.D., Lin, L.C., Chen, C.P., et al., 2010. Sex differences in high-fat diet-induced obesity, metabolic alterations and learning, and synaptic plasticity deficits in mice. Obesity (Silver Spring) 18(3):463—469.

[7] Regitz-Zagrosek, V., Lehmkuhl, E., Weickert, M.O., 2006. Gender differences in the metabolic syndrome and their role for cardiovascular disease. Clinical Research in Cardiology 95(3):136—147.

[8] Park, Y.W., Zhu, S., Palaniappan, L., Heshka, S., Carnethon, M.R., Heymsfield, S.B., 2003. The metabolic syndrome: prevalence and associated risk factor findings in the US population from the Third National Health and Nutrition Examination Survey, 1988-1994. Archives of Internal Medicine 163(4):427—436.

[9] Carr, M.C., 2003. The emergence of the metabolic syndrome with menopause. Journal of Clinical Endocrinology & Metabolism 88(6):2404—2411.

[10] Thurston, R.C., Sowers, M.R., Sternfeld, B., Gold, E.B., Bromberger, J., Chang, Y., et al., 2009. Gains in body fat and vasomotor symptom reporting over the menopausal transition: the study of women's health across the nation. American Journal of Epidemiology 170(6):766—774.

[11] Liu, P., Ji, Y., Yuen, T., Rendina-Ruedy, E., DeMambro, V.E., Dhawan, S., et al., 2017. Blocking FSH induces thermogenic adipose tissue and reduces body fat. Nature 546(7656):107—112.

[12] Li, X., Chen, W., Li, P., Wei, J., Cheng, Y., Liu, P., et al., 2017. Follicular stimulating hormone accelerates atherogenesis by increasing endothelial VCAM-1 expression. Theranostics 7(19):4671—4688.

[13] Jones, M.E., Thorburn, A.W., Britt, K.L., Hewitt, K.N., Wreford, N.G., Proietto, J., et al., 2000. Aromatase-deficient (ArKO) mice have a phenotype of increased adiposity. Proceedings of the National Academy of Sciences of the United States of America 97(23):12735—12740.

[14] Gao, H., Bryzgalova, G., Hedman, E., Khan, A., Efendic, S., Gustafsson, J.A., et al., 2006. Long-term administration of estradiol decreases expression of hepatic lipogenic genes and improves insulin sensitivity in ob/ob mice: a possible mechanism is through direct regulation of signal transducer and activator of transcription 3. Molecular Endocrinology 20(6):1287—1299.

[15] Kuiper, G.G., Enmark, E., Pelto-Huikko, M., Nilsson, S., Gustafsson, J.A., 1996. Cloning of a novel receptor expressed in rat prostate and ovary. Proceedings of the National Academy of Sciences of the United States of America 93(12): 5925—5930.

[16] Jensen, E.V., DeSombre, E.R., 1973. Estrogen-receptor interaction. Science 182(4108):126—134.

[17] Kuiper, G.G., Carlsson, B., Grandien, K., Enmark, E., Häggblad, J., Nilsson, S., et al., 1997. Comparison of the ligand binding specificity and transcript tissue distribution of estrogen receptors alpha and beta. Endocrinology 138(3):863—870.

[18] Barros, R.P., Gustafsson, J., 2011. Estrogen receptors and the metabolic network. Cell Metabolism 14(3):289—299.

[19] Hevener, A.L., Zhou, Z., Moore, T.M., Drew, B.G., Ribas, V., 2018. The impact of ERα action on muscle metabolism and insulin sensitivity - strong enough for a man, made for a woman. Mol Metab 15:20—34.

[20] Ribas, V., Drew, B.G., Zhou, Z., Phun, J., Kalajian, N.Y., Soleymani, T., et al., 2016. Skeletal muscle action of estrogen receptor α is critical for the maintenance of mitochondrial function and metabolic homeostasis in females. Science Translational Medicine 8(334):334ra354.

[21] Shi, H., Kumar, S.P., Liu, X., 2013. G protein-coupled estrogen receptor in energy homeostasis and obesity pathogenesis. Progress in Molecular Biology and Translational Science 114:193—250.

[22] Ribas, V., Nguyen, M.T., Henstridge, D.C., Nguyen, A.K., Beaven, S.W., Watt, M.J., et al., 2010. Impaired oxidative metabolism and inflammation are associated with insulin resistance in ERalpha-deficient mice. American Journal of Physiology. Endocrinology and Metabolism 298(2):E304—E319.

[23] Deng, J.Y., Hsieh, P.S., Huang, J.P., Lu, L.S., Hung, L.M., 2008. Activation of estrogen receptor is crucial for resveratrol-stimulating muscular glucose uptake via both insulin-dependent and -independent pathways. Diabetes 57(7): 1814—1823.

[24] Huang, E.J., Reichardt, L.F., 2001. Neurotrophins: roles in neuronal development and function. Annual Review of Neuroscience 24:677—736.

[25] Huang, E.J., Reichardt, L.F., 2003. Trk receptors: roles in neuronal signal transduction. Annual Review of Biochemistry 72:609—642.

[26] Markus, A., Patel, T.D., Snider, W.D., 2002. Neurotrophic factors and axonal growth. Current Opinion in Neurobiology 12(5):523—531.

[27] Numakawa, T., Suzuki, S., Kumamaru, E., Adachi, N., Richards, M., Kunugi, H., 2010. BDNF function and intracellular signaling in neurons. Histology & Histopathology 25(2):237—258.

[28] Andres-Alonso, M., Ammar, M.R., Butnaru, I., Gomes, G.M., Acuña Sanhueza, G., Raman, R., et al., 2019. SIPA1L2 controls trafficking and local signaling of TrkB-containing amphisomes at presynaptic terminals. Nature Communications 10(1):5448.

[29] Shen, J., Ghai, K., Sompol, P., Liu, X., Cao, X., Iuvone, P.M., et al., 2012. N-acetyl serotonin derivatives as potent neuroprotectants for retinas. Proceedings of the National Academy of Sciences of the United States of America 109(9):3540—3545.

[30] Kernie, S.G., Liebl, D.J., Parada, L.F., 2000. BDNF regulates eating behavior and locomotor activity in mice. The EMBO Journal 19(6):1290—1300.

[31] Unger, T.J., Calderon, G.A., Bradley, L.C., Sena-Esteves, M., Rios, M., 2007. Selective deletion of Bdnf in the ventromedial and dorsomedial hypothalamus of adult mice results in hyperphagic behavior and obesity. Journal of Neuroscience 27(52):14265—14274.

[32] Yang, X., Brobst, D., Chan, W.S., Tse, M.C.L., Herlea-Pana, O., Ahuja, P., 2019. Muscle-generated BDNF is a sexually dimorphic myokine that controls metabolic flexibility. Science Signaling 12(594):eaau1468.

Original Article

[33] Poduslo, J.F., Curran, G.L., 1996. Permeability at the blood-brain and blood-nerve barriers of the neurotrophic factors: NGF, CNTF, NT-3, BDNF. Brain Res Mol Brain Res 36(2):280–286.

[34] Jang, S.W., Liu, X., Yepes, M., Shepherd, K.R., Miller, G.W., Liu, Y., et al., 2010. A selective TrkB agonist with potent neurotrophic activities by 7,8-dihydroxyflavone. Proceedings of the National Academy of Sciences of the United States of America 107(6):2687–2692.

[35] Chen, Y., Zhao, Z., Xia, G., Xue, F., Chen, C., Zhang, Y., 2020. Fabrication and characterization of zein/lactoferrin composite nanoparticles for encapsulating 7,8-dihydroxyflavone: enhancement of stability, water solubility and bio-accessibility. International Journal of Biological Macromolecules 146:179–192.

[36] Chen, C., Wang, Z., Zhang, Z., Liu, X., Kang, S.S., Zhang, Y., et al., 2018. The prodrug of 7,8-dihydroxyflavone development and therapeutic efficacy for treating Alzheimer's disease. Proceedings of the National Academy of Sciences of the United States of America 115(3):578–583.

[37] García-Díaz Barriga, G., Giralt, A., Anglada-Huguet, M., Gaja-Capdevila, N., Orlandi, J.G., Soriano, J., et al., 2017. 7,8-dihydroxyflavone ameliorates cognitive and motor deficits in a Huntington's disease mouse model through specific activation of the PLCγ1 pathway. Human Molecular Genetics 26(16):3144–3160.

[38] Amin, N., Xie, S., Tan, X., Chen, Y., Ren, Q., Botchway, B.O.A., et al., 2020. Optimized integration of fluoxetine and 7, 8-dihydroxyflavone as an efficient therapy for reversing depressive-like behavior in mice during the perimenopausal period. Progress In Neuro-Psychopharmacology & Biological Psychiatry 101:109939.

[39] Sconce, M.D., Churchill, M.J., Moore, C., Meshul, C.K., 2015. Intervention with 7,8-dihydroxyflavone blocks further striatal terminal loss and restores motor deficits in a progressive mouse model of Parkinson's disease. Neuroscience 290:454–471.

[40] Choi, J.W., Lee, C.W., Lee, J., Choi, D.J., Sohng, J.K., Park, Y.I., 2016. 7,8-Dihydroxyflavone inhibits adipocyte differentiation via antioxidant activity and induces apoptosis in 3T3-L1 preadipocyte cells. Life Sciences 144:103–112.

[41] Kumar, D., Dwivedi, D.K., Lahkar, M., Jangra, A., 2019. Hepatoprotective potential of 7,8-Dihydroxyflavone against alcohol and high-fat diet induced liver toxicity via attenuation of oxido-nitrosative stress and NF-κB activation. Pharmacological Reports 71(6):1235–1243.

[42] Chan, C.B., Tse, M.C., Liu, X., Zhang, S., Schmidt, R., Otten, R., et al., 2015. Activation of muscular TrkB by its small molecular agonist 7,8-dihydroxyflavone sex-dependently regulates energy metabolism in diet-induced obese mice. Chemical Biology 22(3):355–368.

[43] Wood, J., Tse, M.C.L., Yang, X., Brobst, D., Liu, Z., Pang, B.P.S., et al., 2018. BDNF mimetic alleviates body weight gain in obese mice by enhancing mitochondrial biogenesis in skeletal muscle. Metabolism Clinical and Experimental 87:113–122.

[44] Cikla, U., Chanana, V., Kintner, D.B., Udho, E., Eickhoff, J., Sun, W., et al., 2016. ERα signaling is required for TrkB-mediated hippocampal neuroprotection in female neonatal mice after hypoxic ischemic encephalopathy(1,2,3). eNeuro 3(1):e0025.

[45] Jaric, I., Rocks, D., Greally, J.M., Suzuki, M., Kundakovic, M., 2019. Chromatin organization in the female mouse brain fluctuates across the oestrous cycle. Nature Communications 10(1):2851.

[46] McLean, A.C., Valenzuela, N., Fai, S., Bennett, S.A., 2012. Performing vaginal lavage, crystal violet staining, and vaginal cytological evaluation for mouse estrous cycle staging identification. Journal of Visualized Experiments 67:e4389.

[47] Judex, S., Luu, Y.K., Ozcivici, E., Adler, B., Lublinsky, S., Rubin, C.T., 2010. Quantification of adiposity in small rodents using micro-CT. Methods 50(1):14–19.

[48] Khandaker, M., Riahinezhad, S., Williams, W.R., Wolf, R., 2017. Microgroove and collagen-poly(ε-caprolactone) nanofiber mesh coating improves the mechanical stability and osseointegration of titanium implants. Nanomaterials (Basel) 7(6):145.

[49] Brown, C., LaRocca, J., Pietruska, J., Ota, M., Anderson, L., Smith, S.D., et al., 2010. Subfertility caused by altered follicular development and oocyte growth in female mice lacking PKB alpha/Akt1. Biology of Reproduction 82(2):246–256.

[50] Johnson, J., Canning, J., Kaneko, T., Pru, J.K., Tilly, J.L., 2004. Germline stem cells and follicular renewal in the postnatal mammalian ovary. Nature 428(6979):145–150.

[51] Perez, G.I., Robles, R., Knudson, C.M., Flaws, J.A., Korsmeyer, S.J., Tilly, J.L., 1999. Prolongation of ovarian lifespan into advanced chronological age by Bax-deficiency. Nature Genetics 21(2):200–203.

[52] Morita, Y., Perez, G.I., Maravei, D.V., Tilly, K.I., Tilly, J.L., 1999. Targeted expression of Bcl-2 in mouse oocytes inhibits ovarian follicle atresia and prevents spontaneous and chemotherapy-induced oocyte apoptosis in vitro. Molecular Endocrinology 13(6):841–850.

[53] Livak, K.J., Schmittgen, T.D., 2001. Analysis of relative gene expression data using real-time quantitative PCR and the 2(-Delta Delta C(T)) Method. Methods 25(4):402–408.

[54] Brenachot, X., Ramadori, G., Ioris, R.M., Veyrat-Durebex, C., Altirriba, J., Aras, E., et al., 2017. Hepatic protein tyrosine phosphatase receptor gamma links obesity-induced inflammation to insulin resistance. Nature Communications 8(1):1820.

[55] Barzilai, N., Huffman, D.M., Muzumdar, R.H., Bartke, A., 2012. The critical role of metabolic pathways in aging. Diabetes 61(6):1315–1322.

[56] López-Otín, C., Blasco, M.A., Partridge, L., Serrano, M., Kroemer, G., 2013. The hallmarks of aging. Cell 153(6):1194–1217.

[57] Jiang, Y., Zhang, Z., Cha, L., Li, L., Zhu, D., Fang, Z., et al., 2019. Resveratrol plays a protective role against premature ovarian failure and prompts female germline stem cell survival. International Journal of Molecular Sciences 20(14):3605.

[58] Hakansson, A., Molin, G., 2011. Gut microbiota and inflammation. Nutrients 3(6):637–682.

[59] Cannon, B., Nedergaard, J., 2004. Brown adipose tissue: function and physiological significance. Physiological Reviews 84(1):277–359.

[60] Anbalagan, M., Rowan, B.G., 2015. Estrogen receptor alpha phosphorylation and its functional impact in human breast cancer. Molecular and Cellular Endocrinology 418(Pt 3):264–272.

[61] Barletta, F., Wong, C.W., McNally, C., Komm, B.S., Katzenellenbogen, B., Cheskis, B.J., 2004. Characterization of the interactions of estrogen receptor and MNAR in the activation of cSrc. Molecular Endocrinology 18(5):1096–1108.

[62] Mao, C., Livezey, M., Kim, J.E., Shapiro, D.J., 2016. Antiestrogen resistant cell lines expressing estrogen receptor α mutations upregulate the unfolded protein response and are killed by BHPI. Scientific Reports 6:34753.

[63] Zeng, M., Li, M., Li, M., Zhang, B., Li, B., Zhang, L., et al., 2018. 2-Phenylacetamide isolated from the seeds of lepidium apetalum and its estrogen-like effects in vitro and in vivo. Molecules 23(9):2293.

[64] Belisle, S., Bellabarba, D., Lehoux, J.G., 1985. On the presence of nonfunctional uterine estrogen receptors in middle-aged and old C57BL/6J mice. Endocrinology 116(1):148–153.

[65] Vandenberg, L.N., Welshons, W.V., Vom Saal, F.S., Toutain, P.L., Myers, J.P., 2014. Should oral gavage be abandoned in toxicity testing of endocrine disruptors? Environmental Health 13(1):46.

[66] Cao, J., Rebuli, M.E., Rogers, J., Todd, K.L., Leyrer, S.M., Ferguson, S.A., et al., 2013. Prenatal bisphenol A exposure alters sex-specific estrogen receptor expression in the neonatal rat hypothalamus and amygdala. Toxicological Sciences 133(1):157–173.

[67] Ovadya, Y., Landsberger, T., Leins, H., Vadai, E., Gal, H., Biran, A., et al., 2018. Impaired immune surveillance accelerates accumulation of senescent cells and aging. Nature Communications 9(1):5435.

[68] Pechenino, A.S., Lin, L., Mbai, F.N., Lee, A.R., He, X.M., Stallone, J.N., et al., 2011. Impact of aging vs. estrogen loss on cardiac gene expression: estrogen replacement and inflammation. Physiological Genomics 43(18):1065—1073.

[69] Pfeilschifter, J., Köditz, R., Pfohl, M., Schatz, H., 2002. Changes in proinflammatory cytokine activity after menopause. Endocrine Reviews 23(1):90—119.

[70] Hoyles, L., Snelling, T., Umlai, U.K., Nicholson, J.K., Carding, S.R., Glen, R.C., et al., 2018. Microbiome-host systems interactions: protective effects of propionate upon the blood-brain barrier. Microbiome 6(1):55.

[71] Chen, C., Ahn, E.H., Kang, S.S., Liu, X., Alam, A., Ye, K., 2020. Gut dysbiosis contributes to amyloid pathology, associated with C/EBPβ/AEP signaling activation in Alzheimer's disease mouse model. Science Advancement 6:eaba0466.

[72] Chen, Y., Jin, L., Li, Y., Xia, G., Chen, C., Zhang, Y., 2018. Bamboo-shaving polysaccharide protects against high-diet induced obesity and modulates the gut microbiota of mice. Journal of Functional Foods 49:20—31.

[73] Mikołajczyk, A., Złotkowska, D., 2018. Neuroimmunological implications of subclinical lipopolysaccharide from Salmonella enteritidis. International Journal of Molecular Sciences 19(10):3274.

[74] Caesar, R., Tremaroli, V., Kovatcheva-Datchary, P., Cani, P.D., Bäckhed, F., 2015. Crosstalk between gut microbiota and dietary lipids aggravates WAT inflammation through TLR signaling. Cell Metabolism 22(4):658—668.

[75] Shan, C.Y., Yang, J.H., Kong, Y., Wang, X.Y., Zheng, M.Y., Xu, Y.G., et al., 2013. Alteration of the intestinal barrier and GLP2 secretion in Berberine-treated type 2 diabetic rats. Journal of Endocrinology 218(3):255—262.

[76] Shi, H., Kokoeva, M.V., Inouye, K., Tzameli, I., Yin, H., Flier, J.S., 2006. TLR4 links innate immunity and fatty acid-induced insulin resistance. Journal of Clinical Investigation 116(11):3015—3025.

[77] Cui, M., Xiao, H., Li, Y., Zhang, S., Dong, J., Wang, B., et al., 2019. Sexual dimorphism of gut microbiota dictates therapeutics efficacy of radiation injuries. Advancement of Science 6(21):1901048.

[78] Chen, J.Q., Brown, T.R., Russo, J., 2009. Regulation of energy metabolism pathways by estrogens and estrogenic chemicals and potential implications in obesity associated with increased exposure to endocrine disruptors. Biochimica et Biophysica Acta 1793(7):1128—1143.

[79] Lösel, R., Wehling, M., 2003. Nongenomic actions of steroid hormones. Nature Reviews Molecular Cell Biology 4(1):46—56.

[80] Murphy, L.C., Seekallu, S.V., Watson, P.H., 2011. Clinical significance of estrogen receptor phosphorylation. Endocrine-Related Cancer 18(1):R1—R14.

[81] Ward, R.D., Weigel, N.L., 2009. Steroid receptor phosphorylation: assigning function to site-specific phosphorylation. BioFactors 35(6):528—536.

[82] Sun, J., Zhou, W., Kaliappan, K., Nawaz, Z., Slingerland, J.M., 2012. ERα phosphorylation at Y537 by Src triggers E6-AP-ERα binding, ERα ubiquitylation, promoter occupancy, and target gene expression. Molecular Endocrinology 26(9):1567—1577.

[83] Kato, S., Endoh, H., Masuhiro, Y., Kitamoto, T., Uchiyama, S., Sasaki, H., et al., 1995. Activation of the estrogen receptor through phosphorylation by mitogen-activated protein kinase. Science 270(5241):1491—1494.

[84] Bunone, G., Briand, P.A., Miksicek, R.J., Picard, D., 1996. Activation of the unliganded estrogen receptor by EGF involves the MAP kinase pathway and direct phosphorylation. The EMBO Journal 15(9):2174—2183.

[85] Ngan, E.S., Ma, Z.Q., Chua, S.S., DeMayo, F.J., Tsai, S.Y., 2002. Inducible expression of FGF-3 in mouse mammary gland. Proceedings of the National Academy of Sciences of the United States of America 99(17):11187—11192.

[86] Arnold, S.F., Obourn, J.D., Yudt, M.R., Carter, T.H., Notides, A.C., 1995. In vivo and in vitro phosphorylation of the human estrogen receptor. The Journal of Steroid Biochemistry and Molecular Biology 52(2):159—171.

[87] Huang, Y.Z., McNamara, J.O., 2010. Mutual regulation of Src family kinases and the neurotrophin receptor TrkB. Journal of Biological Chemistry 285(11):8207—8217.